

Suggestions for revision or reasons for rejection (will be published if the paper is accepted for final publication)

In the revised manuscript, description of the experiments, analysis methods, and discussion are much improved from original version. I appreciate the authors' great effort for improving their draft according to reviewers' comments. I only have a few minor comments.

Reply: Thank you for your affirmation. We appreciate your constructive comments to improve our work.

1. Figure 13 is the key for mentioning inter-model difference in land configuration (land-sea mask) and simulated results. In Figure A of "response to reviewers", the authors showed each model's land/ocean mask. This should also be shown in Figure 13. I mean, coastlines shown in Fig. 13 should be consistent with Fig. A. I found that land area fraction data, sftlf, is available at CERA website.

<https://cera-www.dkrz.de/WDCC/ui/cerasearch/q?page=0&query=sftlf+lgm&rows=15>

In addition, please include Figure A into supplementary information. This is really important for mentioning inter-model consistency/difference in LGM SST gradient.

Reply: Thank you very much for providing the information of the dataset. We downloaded the land area fraction data and used in Fig. 13 for each model. And Fig. A is added as Fig. S9 in the revised version.

2. The description of model and sensitivity experiments explained in discussion section should be included in section 2. I mean, the subsection title of 2.1 should be modified (e.g. PMIP3 models and experiments), then new subsection (the NESM model experiments) should be added.

Reply: The new subsection has been added as Sec. "2.2 NESM model and experiments" in the revised version, and the section numbers have been changed accordingly.

3. >> Figures S1 and S2 seem identical to Figures 2 and 1 of Yan et al. (2016). You may need any copyright permission from Springer-Nature.

> Reply: The paper of Yan et al. (2016) has been purchased "Open Access" in Climate Dynamics. So, we don't need to obtain the copyright.

Even though it is open access, you should refer that paper in the figure caption. E.g. "reprint of Fig. XX of Yan et al. (2016)."

Reply: Thank you for pointing out this. We have added the reference in the figure caption of Figure S1 and S2.

Suggestions for revision or reasons for rejection (will be published if the paper is accepted for final publication)

Review of revised manuscript: "Understanding the Australian monsoon change during the Last Glacial Maximum with multi-model ensemble" by Yan et al.

General comments:

The authors have gone to some effort to address reviewer comments on the manuscript. The revised manuscript now includes a more satisfactory decomposition of the rainfall changes based on Huang et al. (2013) approach using changes in specific humidity and vertical motion. The paper also now addresses the extent to which models agree on changes as well as presenting multi-model mean results.

I therefore recommend publication subject to minor corrections outlined below. (Please note that the manuscript would benefit from further proof-reading as I have not provided an exhaustive list of corrections.)

Reply: Thank you for your affirmation and careful corrections. We have gone through carefully and made corrections.

Specific Comments:

1. Line 27: replace "multi-models' experiments" with "multi-model experiments"

Reply: Changed. Line 27.

2. Line 34: delete "the" before northern Australia.

Reply: Deleted. Line 34.

3. Line 130: while CMIP5 models have reasonable performance simulating the Australian monsoon precipitation, there are some biases, e.g. some models are much too wet or dry, or fail to simulate the reversal of winds. This is discussed in the Jourdain (2013) and Brown (2016) papers cited here. Please provide a more balanced assessment of model skill in simulating the Australian monsoon.

Reply: We have changed the statement in the revised version. Lines 147-152.

4. Line 168: Huang et al. (2013) argue that T_{adv} term can be neglected in the tropics to simplify the analysis. Is there a reason not to neglect this term?

Reply: The T_{adv} term listed here comes from the EQ. (3), we didn't make further simplification. But yes, actually this term could be negligible as seen in the Fig. S3 and Fig. S6.

5. Line 183-184: I am not sure what this sentence means. Are you arguing that the exact definition of the monsoon domain is not important for the results? Or that the analysis presented in the rest of the paper does not use this domain?

Reply: We mean that the analysis presented in the rest of the paper does not consider this domain. We added a statement in the revised version to make it easy to understand. Line 194.

6. Line 226: "rest terms"? do you mean "the rest of the terms"?

Reply: Yes, it means "the rest terms of the equation (4)". Changed in the revised version. Line 236.

7. Line 229 (Figure S3): Why do the terms not sum to give the total rainfall change? Also, note comment 4 above about neglecting the advection term.

Reply: The actual precipitation changes are nonlinear, so the linear sum of the terms might not meet the actual change. And yes, we confirm that the advection term is negligible.

8. Line 298: "Thermal effects" should be "thermodynamic effects" (here and in other places, e.g. lines 324, 414, 415).

Reply: All changed in the revised version. Lines 267, 308, 336, 424, 426.

9. Line 299: Replace "impact" with "magnitude" (i.e. quantitative comparison).

Reply: Changed. Line 309.

10. Line 309: Remove brackets?

Reply: Yes, thank you for pointing out this mistake. Changed in the revised version. Line 319.

11. Line 314: Replace "which is consists with our work in this point of view" with "which is also consistent with our work".

Reply: Changed. Line 325.

12. Line 316: Remind the reader what is shown by the reconstruction of Liu et al. (2015).

Reply: Yes, added in the revised version. Lines 327-328.

13. Line 330-351: This paragraph is a bit confusing. Perhaps remove some of the detail, e.g. lines 338-346. Also it needs careful proof reading for both English and for the scientific content of the discussion. Several different points are being mixed together, and the last two sentences (347-351) seem out of place.

Reply: We are trying to discuss the effect of the orbital induced insolation changes, which has different impacts on different hemisphere due to the different heat capacity of the land and the ocean. And find that the insolation change is not the main forcing that influences Australian monsoon precipitation change. Yes, some details can be removed. Lines 342-362.

14. Line 331: insert "relative to the present day" after November.

Reply: Added in the revised version. Line 343.

15. Line 334: delete "of" before "the ocean".

Reply: Deleted. Line 347.

16. Line 365: replace "synthesis" with "hypothesis".

Reply: Changed. Line 376.

17. Line 378: replace "sensitive" with "sensitivity"

Reply: The related "sensitive experiment" have all been changed with "sensitivity" in the revised version. Lines 86, 154, 158, 385, 436, 442.

18. Line 379: replace "to be" with "are"

Reply: Changed. Line 386.

19. Line 385: replace "wind filed" with "wind field"

Reply: Changed. Line 393.

20. Line 395: replace "East Pacific... patter" with "eastern Pacific El Nino-like pattern".

Reply: Changed. Line 403.

21. Lines 414, 415: thermodynamic not thermal

Reply: All changed in the revised version. Lines 267, 308, 336, 424, 426.

22. Line 425, 431: sensitivity not sensitive

Reply: All changed. Lines 86, 154, 158, 385, 436, 442.

23. Line 440-441: I would argue that this will not "improve model performance", but instead increase confidence in model results or understanding of model-data disagreement. Changes in the model physics, resolution etc. are required to improve model performance – a different matter entirely.

Reply: Yes, you are right. We have changed the statement. Lines 451-452.

1 **Understanding the Australian Monsoon change during the Last Glacial Maximum**
2 **with multi-model ensemble**

3 **Mi Yan^{1,2}, Bin Wang^{3,4}, Jian Liu^{1,2*}, Axing Zhu^{1,2,5,6}, Liang Ning^{1,2,7} and Jian Cao⁴**

4 1 Key Laboratory of Virtual Geographic Environment, Ministry of Education; State key
5 Laboratory of Geographical Environment Evolution, Jiangsu Provincial Cultivation Base; School
6 of Geography Science, Nanjing Normal University, Nanjing, 210023, China.

7 2 Jiangsu Center for Collaborative Innovation in Geographical Information Resource
8 Development and Application, Nanjing, 210023, China.

9 3 Department of Atmospheric Sciences, University of Hawaii at Manoa, Honolulu, HI 96825,
10 USA.

11 4 Earth System Modeling Center, Nanjing University of Information Science and Technology,
12 Nanjing, 210044, China.

13 5 State Key Lab of Resources and Environmental Information System, Institute of Geographic
14 Sciences and Natural Resources Research, Chinese Academy of Sciences, Beijing, 100101,
15 China

16 6 Department of Geography, University of Wisconsin-Madison, Madison, WI 53706, USA

17 7 Climate System Research Center, Department of Geosciences, University of Massachusetts,
18 Amherst, 01003, USA.

19
20 * Corresponding author address: Dr. Jian Liu, School of Geography Science, Nanjing Normal
21 University, 1 Wenyuan Road, Nanjing 210023, China

22 E-mail: jliu@njnu.edu.cn

Abstract

The response of Australian monsoon to the external forcings and the related mechanisms during the Last Glacial Maximum (LGM) is investigated by multi-models² experiments in CMIP5/PMIP3. Although the annual mean precipitation over the Australian monsoon region decreases, the annual range, or the monsoonality, is enhanced. The precipitation increases in early austral summer and decreases in austral winter, resulting in the amplified annual range, but the main contribution comes from the decreased precipitation in austral winter. The decreased winter precipitation is primarily caused by weakened upward motion, although reduced water vapor has also a moderate contribution. The weakened upward motion is induced by the enhanced land–sea thermal contrast, which intensifies the divergence over ~~the~~ northern Australia. The increased Australian monsoon rainfall in early summer, on the other hand, is an integrated result of the positive effect of local dynamic processes (enhanced moisture convergence) and the negative effect of thermodynamics (reduced moisture content). The enhanced moisture convergence is caused by two factors: the strengthened northwest–southeast thermal contrast between the cooler Indochina–western Indonesia and the warmer northeastern Australia, and the east–west sea surface temperature gradients between the warmer western Pacific and cooler eastern Indian Ocean, both due to the alteration of land–sea configuration arising from the sea level drop. The enhanced Australian monsoonality in the LGM is not associated with global scale circulation change such as the shift of the ITCZ, rather, it is mainly due to the change of regional circulations around Australia arising from the changes in land-sea contrast and the east-west SST gradients over the Indo-western Pacific oceans. This finding should be taken into account when investigating its future change under global warming. Our findings may also explain why proxy records indicate different changes in Australian monsoon precipitation during the LGM.

49 **1 Introduction**

50 The changes of the Australian monsoon are crucial for human society and ecology in
51 Australia (Reeves et al., 2013a), considering the socio-economic importance of monsoon rainfall
52 (Wang et al., 2017). As the monsoons of the summer hemisphere are linked via outflows from
53 the opposing winter hemisphere, the Australian monsoon can also influence the Asian–
54 Indonesian–Australian monsoon system (Eroglu et al., 2016). It is important to understand how
55 and why the Australian monsoon would change in response to global climate change.

56 With strong climatic forcings (including low greenhouse gas (GHG) concentrations, large
57 ice-sheets, and low sea level, etc.), the Last Glacial Maximum (LGM) is one of the key periods
58 that provides an opportunity to better understand the mechanisms of how global and regional
59 climate respond to external forcings (Hewitt et al., 2001; Braconnot et al., 2007; Braconnot et al.,
60 2011; Harrison et al., 2014). Previous studies have investigated how the external forcing and
61 boundary conditions during the LGM affected the Intertropical Convergence Zone (ITCZ)
62 (Broccoli et al., 2006; Donohoe et al., 2013; McGee et al., 2014), the Walker circulation
63 (DiNezio et al., 2011), the Indo-Pacific climate (Xu et al., 2010; DiNezio and Tierney, 2013;
64 DiNezio et al., 2016), the SH circulation (Rojas, 2013), and the global monsoon (Jiang et al.,
65 2015; Yan et al., 2016). The Australian monsoon onset and variability during the post-glacial, the
66 late deglaciation, and the Holocene have also been studied using proxy datasets (Ayliffe et al.,
67 2013; De Deckker et al., 2014; Kuhnt et al., 2015; Bayon et al., 2017). However, due to the
68 limitation of the scarce proxy datasets, the Australian monsoon change during the LGM is far
69 from clearly understood.

70 There are different proxy evidences indicating different Australian monsoon change
71 during the LGM. Here, the Australian monsoon intensity is represented by the seasonality of
72 precipitation, i.e., a stronger monsoon means a wetter summer and/or drier winter. Some records
73 show wet conditions over Australia during the LGM (Ayliffe et al., 2013), while other proxies
74 indicate drier conditions (Denniston et al., 2013; Denniston et al., 2017; DiNezio and Tierney,
75 2013). The isotopes from eggshell of five regions across Australia affirms that Australia becomes
76 drier in the LGM (Miller et al., 2016), while the archaeological record showed a refugia-type
77 hunter-gatherer response over northwest and northeast Australia during the LGM (Williams et
78 al., 2013), indicating that these areas may have had a wetter summer and were therefore

79 preferred by people as refugia. The synthesis by the OZ-INTIMATE (Australian INTIMATE,
80 INTegration of Ice core, MARine and TERrestrial records) project (Turney et al., 2006; Petherick
81 et al., 2013) showed that the palaeoenvironment over Northern Australia during the LGM was
82 characterized by drier conditions although wet periods were also noted in the fluvial records
83 (Reeves et al., 2013a; Reeves et al., 2013b).

84 The change in the Australian monsoon was inconclusive during the LGM based on proxy
85 data. Therefore, scholars started investigating the Australian monsoon change from numerical
86 simulation perspectives. The sensitivity of Australian monsoon to forcings during the late
87 Quaternary has been analyzed using simulations by Fast Ocean Atmosphere Model (Marshall
88 and Lynch, 2006, 2008). Numerical experiments have been conducted to analyze the impacts of
89 obliquity and precession with a coupled General Circulation Model (Wyrwoll et al., 2007) and
90 orbital time-scale circulation with Community Climate Model (Wyrwoll et al., 2012) on the
91 Australian monsoon. However, different models may have different responses to the same
92 external forcings, such that the simulated results may have model dependence. Multi-model
93 ensemble (MME) can reduce the model biases and therefore provide more reasonable results of
94 how and why climate system responds to the external forcing changes. The MME can also
95 provide a clearer perspective on model uncertainties.

96 Yan et al (2016) thus used the multi-model ensemble approach to examine the response
97 of global monsoon to the LGM conditions. It was found that the global monsoon and most sub-
98 monsoons weakened under the LGM conditions. Some brief hypothesis was made to explain the
99 changes from global and hemispheric perspectives. The Australian monsoon was thought to be
100 strengthened due to the southward shift of the ITCZ resulted from the hemispheric thermal
101 contrast and due to the land-sea thermal contrast resulted from the land-configuration. However,
102 this simulated result of strengthened monsoon or wet condition has not been proved yet. As
103 mentioned above, it is inconclusive whether the Australian monsoon is strengthened or not
104 during the LGM, due to the limitations of proxies' and models' uncertainties. Neither model
105 outputs nor proxy records provide a "true" record of the LGM, as proxy records require
106 interpretation and calibration and may be spatially incomplete, while models contain biases.
107 Therefore, model-data and inter-model comparison are needed and studies on the mechanisms
108 are required to better understand the Australian monsoon change during the LGM. Moreover,
109 some studies show that the Australian climate during the last glacial period was modulated by

110 additional mechanisms rather than simply the ITCZ (Bayon et al., 2017). Thus, single forcing
111 runs are also required to figure out the contributions of different forcings.

112 This paper investigates the Australian monsoon change during the LGM and its
113 mechanisms from both thermodynamics and dynamics perspectives, using the multi-model
114 ensemble mean derived from models in the fifth phase of the Coupled Model Intercomparison
115 Project (CMIP5) (Taylor et al., 2012) and the third phase of the Paleoclimate Modeling
116 Intercomparison Project (PMIP3) (Braconnot et al., 2012). We are also trying to quantify the
117 contributions of the thermodynamic and the dynamic processes to the Australian monsoon
118 change during the LGM. Additionally, we are applying single forcing run to test the effect of
119 land-configuration as mentioned in Yan et al. (2016). The models and experiments used in this
120 paper are introduced in Sect. 2. Section 3 describes simulated results and the physical
121 mechanisms. The comparison with proxies and other simulations is discussed in Sect. 4 and the
122 conclusions are made in Sect. 5.

123

124 **2 Methods**

125 **2.1 CMIP5/PMIP3 Models and experiments**

126 Two experiments performed by models participating in CMIP5/PMIP3 are compared in
127 this paper: the Last Glacial Maximum Experiment (LGME) and the pre-industrial (PI) control
128 run (piControl). The models and experiments are listed in Table 1, including 7 models and 2
129 experiments. ~~The models contributed to CMIP5 have been evaluated in the previous studies to
130 have good performance in simulating the Australian monsoon precipitation seasonality or
131 seasonal cycle (Jourdain et al., 2013; Brown et al., 2016), which is used to represent the
132 Australian monsoon intensity in this study.~~

133 The last 100 years of the LGME and the last 500 years of the piControl from each model
134 are used to illustrate the model climatology. To obtain the multi-model ensemble (MME), the
135 model outputs were interpolated into a fixed 2.5° (latitude) \times 2.5° (longitude) grid using the
136 bilinear interpolation method.

137 The LGM external forcing and boundary conditions are listed in Table 2. More specific
138 documentation can be found on the PMIP3 website (<https://pmip3.lsce.ipsl.fr>). Compared with

139 the PI, during the LGM the Southern Hemisphere (SH) low latitudes (30°S-EQ) receive more
140 insolation from January to August and less from August to December. The NH low latitudes
141 (EQ-30°N) receive less insolation from June to October and more from November to May (Fig.
142 S1). Due to the decreased sea level, the landmasses expanded during the LGM. A land bridge
143 formed between Indochina and western Indonesia, and the Arafura Sea between New Guinea and
144 Australia closed and became landmass (Fig. S2).

145 To illustrate the robust changes simulated by the different models, the signal-to-noise
146 ratio (S2N) test is used. The S2N is defined by the ratio of the absolute mean of the MME (as the
147 signal) to the averaged absolute deviation of the individual model against the MME (as the
148 noise) (Yan et al., 2016). In the following sections, we only consider the areas in which the S2N
149 ratio exceeds one when we examine the differences between the LGME and piControl derived
150 from the MME.

151 The models contributed to CMIP5 have been evaluated in the previous studies to have
152 better performance than those in the CMIP Phase 3 (CMIP3) in simulating the Australian
153 monsoon precipitation seasonality or seasonal cycle (Jourdain et al., 2013; Brown et al., 2016),
154 which is used to represent the Australian monsoon intensity in this study. However, we need to
155 keep in mind that there are large uncertainties in model simulations, which require careful
156 model-data comparison and inter-model comparison.

157 2.2 NESM model and experiments

158 To isolate the impacts of land-sea configuration change, ~~o test this synthesis, we~~
159 conducted two additional sensitivity experiments are conducted using a newly developed fully
160 coupled earth system model, the Nanjing University of Information Science and Technology
161 Earth System model version 1 (NESM v1, Cao et al., 2015). One is the ~~The piControl PI control~~
162 run (NESM PI), which is designed the same as the PMIP3 protocol. The other is the land sea
163 configuration sensitive sensitivity run (NESM LSM), which is designed the same as the
164 piControl NESM PI but with the LGM land sea configuration. The two experiments are run 500
165 years after spin-up, and the last 100 years are used.

166 2.2-3 Decomposition method

带格式的: 缩进: 首行缩进: 0 厘米

带格式的: 首行缩进: 3 字符

167 For attribution of precipitation changes, we use a simplified relation based on the
 168 linearized equation of moisture budget used in the previous works (Chou et al., 2009; Seager et
 169 al., 2010; Huang et al., 2013; Endo and Kitoh, 2014; Liu et al., 2016). Considering a quasi-
 170 equilibrium state, the vertical integrated moisture conservation can be written as:

$$- \int_{1000}^0 \nabla \cdot (q \vec{v}) dp = P - E \quad (1)$$

172 where q is specific humidity, \vec{v} is horizontal velocity, p is pressure, P is precipitation, and E is
 173 the surface evaporation. Since water vapor is concentrated in the lower troposphere, the vertical
 174 integrated total column moisture divergence can be approximately replaced by the integration
 175 from the surface to 500 hPa. Define the $\Delta(\cdot)$ as the change from PI to the LGM, i.e.,

$$\Delta(\cdot) = (\cdot)_{\text{LGM}} - (\cdot)_{\text{PI}} \quad (2)$$

177 Then the precipitation change ΔP can be calculated as follows:

$$\Delta P = - \int_{p_{1000}}^{p_{500}} \Delta(q \cdot \nabla \vec{v}) dp - \int_{p_{1000}}^{p_{500}} \Delta(\vec{v} \cdot \nabla q) dp + \Delta E \quad (3)$$

179 To further simplify the equation, we use $-\omega_{500}$ to represent vertical integrated $\nabla \vec{v}$, and q at the
 180 surface to represent vertical integrated specific humidity (Huang et al., 2013). Thus, the
 181 precipitation change (ΔP) can be represented as

$$\Delta P \propto \bar{\omega}_{500} \cdot \Delta q + \bar{q} \cdot \Delta \omega_{500} + \Delta E - \Delta T_{adv} \quad (4)$$

183 where $\bar{\omega}_{500}$ is 500 hPa vertical velocity in PI, \bar{q} is surface specific humidity in PI, ΔT_{adv} is the
 184 changes due to the moisture advection ($\int_{p_0}^{p_{500}} \Delta(\vec{v} \cdot \nabla q) dp$).

185 The first term in the right-hand side of (4) ($\bar{\omega}_{500} \cdot \Delta q$) represents thermodynamic effect
 186 (due to the change of q), and the second term ($\bar{q} \cdot \Delta \omega_{500}$) represents dynamic effect (due to the
 187 change of circulation).

188 2.3.4 Monsoon domain

189 The monsoon domain is defined following the hydroclimate definition, i.e., a contrast
 190 between wet summer and dry winter (Wang and Ding 2008). The monsoon domain is defined by
 191 the area where the annual range (local summer minus local winter) exceeds 2.0 mm/day, and the
 192 local summer precipitation exceeds 55% of the annual total precipitation. Here in the ~~southern~~
 193 ~~hemisphere~~SH, summer means November to March and winter means May to September. Since
 194 the domains derived from different models are different, and the changes of domain are also
 195 different, we use the fixed domain derived from the merged Climate Prediction Center Analysis

带格式的: 缩进: 首行缩进: 3 字符

196 of Precipitation (CMAP, Xie and Arkin, 1997) and Global Precipitation Climatology Project
197 (GPCP, Huffman et al., 2009) data.

198 Note that the monsoon domain is shown to give a general view of precipitation change,
199 but not the purpose of this study, i.e. the following analysis are not based on the domain.

200

201 **3 Results**

202 We defined the difference of precipitation rate between austral summer (DJF) and austral
203 winter (JJA) as the annual range, i.e. the seasonality, to measure the monsoonality of the
204 Australian monsoon. An increased annual range (or seasonality) means a strengthened
205 monsoonality. Unlike the South African and South American monsoon regions (not shown), the
206 monsoonality of the Australian monsoon derived from the seven models' multi-model ensemble
207 (7MME) is strengthened during the LGM (Fig. 1a). This amplified annual range is the result of
208 increased precipitation in austral summer and decreased precipitation in austral winter (Fig. 1b).
209 Note that the largest decrease in precipitation ~~occurred~~ occurs from April to July (late autumn to
210 early winter), not exactly in austral winter; and the largest increase of precipitation ~~occurred~~
211 occurs in November and December (ND), i.e., austral early summer. Since the amount of
212 autumn–winter reduction of precipitation exceeds the increased precipitation in early summer,
213 the annual mean precipitation over the strengthened annual range region decreases (by 0.36
214 mm/day). In summary, while the total annual precipitation decreases in the LGM, the annual
215 range (or the seasonality) of the Australian monsoon rainfall is amplified due to seasonal
216 redistribution of the precipitation, especially the drying in austral autumn (April–May) and
217 winter (JJA) over Australia.

218 Although there are model biases, most of the models (except MPI-ESM-P) simulate an
219 enhanced annual range (or seasonality/monsoonality) in the central Australian monsoon region
220 (20 °S–5 °S, 120 °E–145 °E) (Table 3 and Fig. 1c). Most of the models (except CNRM-CM5 and
221 MPI-ESM-P) also simulate an increased summer precipitation over that region. All the models
222 simulate decreased precipitation from April to September (Fig. 1c). On the other hand, the
223 simulated annual mean precipitation is decreased in most models, except GISS-E2-R. The model
224 uncertainties will be discussed later in Sec. 4.

225 3.1 Reasons for the decreased precipitation during the LGM in austral winter (JJA)

226 During the LGM, the lower GHG concentration and the large ice-sheets are the primary
227 causes for the decreased global temperature and ~~the~~ humidity. The global surface specific
228 humidity is reduced by 2 g/kg (or 20 %) in JJA during the LGM, compared with the PI. For the
229 SH monsoon regions, the surface specific humidity is reduced more over the Australian monsoon
230 region than over the other two monsoon regions of South Africa and South America (Fig. 2).

231 As suggested by the Clausius–Clapeyron relation (C-C relation), one degree of
232 temperature decrease would lead to about a 7 % decrease in the saturation water vapor (Held and
233 Soden, 2006), or roughly the same scale of decrease in the low tropospheric specific humidity. If
234 the circulation, evaporation and advection remains unchanged, the precipitation should also be
235 reduced by 7 % with regard to the equation (4). During the LGM, the simulated near surface air
236 temperature over the central Australian monsoon region (20°S–5°S, 120°E–145°E) decreases
237 significantly by 2.5 K in JJA, which implies a decrease of about 17 % resulted from the C-C
238 relation. However, the simulated precipitation in the LGM is reduced by 1.45 mm/day or 44 %
239 comparing to the PI, which is far beyond the value suggested by the thermodynamic effect
240 (approximately 17 %). This suggests that the majority of the reduction in winter precipitation is
241 due to the changes of ~~the~~ rest terms ~~in~~ of equation (4), including the circulation change
242 (dynamics), the evaporation change and the change due to the advection term. The changes of
243 each terms show that the circulation change plays a dominant role in the precipitation change
244 over Australia (Fig. S3). The change due to the evaporation is also important. The change due to
245 the advection term is negligible.

246 The change of the surface wind field shows a strengthened divergence pattern over the
247 Australian monsoon region (Fig. 3a, vector), which is consistent with the strengthened
248 descending flow over the Australian monsoon region (Fig. 4) and thus the reduced precipitation
249 (Fig. 3a, shading). The JJA mean near surface air temperature shows that the land is cooler than
250 the adjacent ocean around northern Australia (Fig. 5a), which illustrates a strengthened land–sea
251 thermal contrast because the land cools more than the ocean surface during the LGM. This
252 strengthened land–sea contrast leads to a higher sea-level pressure (SLP) over land and lower
253 SLP over ocean in general (Fig. 5b, shading), and thus the outflows from land (Fig. 5b, vector).
254 The geopotential height at 850 hPa also shows the relative pattern that matches the wind change

255 (Fig. S4a). The difference of divergence/convergence field (Fig. 5c) also indicates that the
256 divergence at 850 hPa over ~~the~~ northern Australia is strengthened during the LGM. The vertical
257 velocity at 500 hPa over the central Australian monsoon region (20 °S-5 °S, 120 °E-145 °E)
258 illustrates that the descending flow strengthened by about 48 %.

259 In conclusion, both the dynamic process (increased subsidence) and the thermodynamic
260 process (reduced water vapor content) contribute to the drier winter in the Australian monsoon
261 region, but the local dynamic processes play a dominant role in the reduction of Australian
262 winter precipitation.

263 3.2 Why the precipitation increased in austral early summer (ND)

264 During ND, the LGM minus PI surface wind difference field shows a strengthened
265 convergence pattern over the central northern Australian monsoon region (Fig. 6a, vector), which
266 is consistent with the increased precipitation (Fig. 6a, shading). The vertical velocity at 500 hPa
267 also shows a strengthened ascending flow over this area (Fig. 7). The increased precipitation
268 over the central Australian monsoon region is clearly against the thermodynamic effects of the
269 low GHG concentration and the presence of the ice-sheets, which tends to reduce the
270 precipitation. The 2-m air temperature ~~was~~is decreased by 2.2 K and the surface specific
271 humidity is reduced by 2.6 g/kg (or 16.0 %) over the Australian monsoon region (Fig. 8). The
272 precipitation would decrease by 15.4 % according to the ~~thermal-thermodynamic~~ effect without
273 the circulation change. However, the precipitation over the Australian monsoon region is
274 increased by about 13.0 %. Therefore, the changes in dynamic processes must induce a 29 %
275 increase of precipitation, so that the net increase in precipitation reaches 13 %.

276 There is a cyclonic wind anomaly associated with an anomalous low pressure over the
277 northwest Australia (Fig. 6a and Fig. 9b, vector), accompanied by a strengthened low-level
278 convergence (Fig. 9c), which favors increased precipitation in the Australian monsoon region.
279 The change of the moisture transport (moisture flux) also ~~indicated~~indicates increased moisture
280 transport into northern Australia (not shown). The cyclonic vorticity in northwest Australia is
281 partially caused by the enhanced strong low-level westerlies that prevail north of Australia.

282 We now seek to determine why there ~~was~~is a strengthened low-level westerly with
283 maximum over north of Australia. We first consider the temperature change. The ND mean 2-m
284 air temperature during the LGM shows that the two enlarged landmasses over the Indo-Pacific

285 warm pool region (resulting from the lower sea level) change differently (Fig. 9a). It is cooler
286 over the northwest landmass (western Indonesia–Indochina) and relatively warmer over the
287 southeast landmass (eastern Indonesia–northern Australia). This temperature variation forms a
288 southeast–northwest temperature gradient (Fig. 9a, Fig. S5a, S5b), accompanied by a northwest–
289 southeast SLP gradient (Fig. 9b, Fig. S5c, S5d). The northwest–southeast pressure gradient is
290 stronger in the geopotential height change at 850 hPa (Fig. S4b). The high pressure in the
291 western Indonesia–Indochina is a part of the larger scale enhanced winter monsoon over the
292 South China Sea. This enhanced winter monsoon flows cross the equator from the NH to the SH
293 and turn into strong westerlies due to deflection induced by the Coriolis force. The 850 hPa
294 convergence strengthens over the Australian monsoon region (Fig. 9c), and the corresponding
295 ascending motion at 500 hPa also increases over the Australian monsoon region.

296 Another reason for circulation change is the sea surface temperature (SST) gradient
297 change. The SST anomaly in ND shows a warmer Western Pacific and cooler Eastern Indian
298 Ocean pattern (Fig. 10), indicating a westward temperature gradient (Fig. S5e), and thus an
299 eastward pressure gradient which, in the equatorial region, can directly enhance westerly winds
300 near the northern Australian monsoon region (Fig. 9b). Li et al. (2012) also found that a cold
301 state of the Wharton Basin (100 °E–130 °E, 20 °S–5 °S) was accompanied by anomalous westerlies
302 and cyclonic circulation anomalies in the Australian monsoon region, which were associated
303 with a strong tropical Australian summer monsoon and enhanced rainfall over northeast
304 Australia.

305 In summary, during ND, the enlarged land area due to sea-level drop enhances the land–
306 sea thermal contrast, and forms a northwest–southeast thermal contrast which induces low
307 pressure over northern Australia but high pressure over the adjacent ocean and the Indochina–
308 western Indonesia, leading to the enhanced convergence over northern Australia and thus
309 increasing the early summer monsoon rainfall. The SST gradients between the warm equatorial
310 western Pacific and the relatively cool eastern Indian Ocean during the pre-summer monsoon
311 season also contribute to the strengthened equatorial westerlies and the cyclonic wind anomaly
312 over northern Australia. These dynamic mechanisms have a positive contribution to the early
313 summer precipitation. The thermal-thermodynamic effects have negative contribution to the
314 precipitation change, but with smaller impact magnitude. Therefore, the early summer
315 precipitation over northern Australia increases. We can also tell from the changes of the

316 decomposed terms that the dynamics plays much more important role in the precipitation change
317 over Australia, especially the distribution pattern (Fig. S6). Again, the impacts of evaporation
318 and advection terms are small.

319

320 **4 Discussion**

321 The intensification of the Australian monsoon in this study is measured by the enhanced
322 seasonal difference (or the seasonality) of precipitation, and is particularly attributed to the
323 decreased austral winter precipitation. This is consistent with the reconstructed results by
324 Mohtadi et al. (2011), which indicated that it was not significantly drier in austral summer during
325 the LGM, while ~~(the winter monsoon is weakened was as weak as the modern period)~~. Whereas
326 the annual mean precipitation is decreased, which means the Australian monsoon would be
327 weakened during the LGM when it is measured by the annual mean precipitation. The modeling
328 study by DiNezio et al. (2013) ~~suggests-suggested~~ a decreasing rainfall across northern Australia
329 during the LGM, consistent with the proxy synthesis by stalagmite (Denniston et al., 2017). The
330 decreased rainfall in their work represents the annual mean precipitation, which ~~is~~ also
331 consistent with our work ~~in this point of view~~. On the other hand, the increased rainfall in
332 austral summer in this study is consistent with what has been revealed in the reconstructed work
333 by Liu et al. (2015), ~~which found intense austral summer precipitation over Papua New Guinea~~
334 ~~and North Australia in LGM.~~ -The decreased annual mean precipitation and the intensified
335 seasonality of precipitation over the Australian monsoon region are in agreement with the
336 synthesis from the simulated result by Tharammal et al. (2013) using a set of experiments.

337 For the forcings and mechanisms of the Australian monsoon change during the LGM,
338 there are large changes in four external forcings during the LGM, including the insolation change
339 resulting from the orbital change, the land-sea configuration change, the GHG change and the
340 presence of ice-sheets. The lower GHG concentrations and the presence of ice-sheets are likely
341 to be contributors to the ~~thermal-thermodynamic~~ effect leading to the reduced water vapor and
342 thus the decreased rainfall both in austral winter and early summer. The enlarged the landmasses
343 over western Indonesia and northeastern Australia are essential to the local dynamic processes
344 that influence the rainfall. The low obliquity and high precession during the LGM may be

345 another factor that can affect the rainfall (Liu et al., 2015). However, the impact of the insolation
346 change caused by the orbital change remains unknown.

347 During the LGM, the insolation over tropical region increased from December to June
348 and decreased from July to November relative to the present day (Fig. 11a). In the annual
349 variation, the precipitation responds to the lower tropospheric moisture convergence. The
350 moisture change depends on temperature change while the circulation change depends on surface
351 temperature gradients change. The change of the surface temperature lags insolation changes
352 because ~~of~~ the ocean and land surfaces have heat capacity (thermal inertial). In other words,
353 insolation is a heating rate which equals to temperature change (tendency) but not the
354 temperature itself. Thus the precipitation change would lag the insolation change by about two
355 months, due to the ocean–atmosphere interaction without other processes. ~~For example, the~~
356 ~~change of seasonal distribution of NH monsoon precipitation lagged the change of the NH~~
357 ~~insolation by one month (Yan et al., 2016). Whereas in this study~~ However, the simulated
358 Australian monsoon precipitation is decreased from March to September and increased from
359 November to February (Fig. 11b), quite different from what it would be (i.e., decrease from
360 September to January and increase from February to August). This indicates the insolation
361 change might have little effect on the Australian monsoon precipitation. Meanwhile, the
362 insolation over SH is increased during the LGM from April to August, when Australia is in late
363 autumn and winter. An increased insolation might make land warmer than ocean thus against the
364 climatology, ~~which may be described by (i.e. cooler land and warmer ocean in winter).~~ However,
365 the simulated surface temperature reduced more over Australia than the adjacent oceans (Fig.
366 5a). On the other hand, the synthesis of Wyrwoll et al. (2007) and Liu et al. (2015) indicates the
367 strong convergence rain belt (ITCZ) stays in the north, ~~resulting in more rainfall over Papua New~~
368 ~~Guinea and less rainfall over North Australia~~ during those times with low obliquity and high
369 precession. ~~The rain belt stays, which is~~ a little more northerly than that stays in our study, ~~;~~
370 ~~which~~ These means that the effect of orbital change and thus the insolation change might be
371 suppressed by other factors.

372 Moreover, the paleoclimate records suggest that it was dry and cool in the Indo-Pacific
373 Warm Pool region during the LGM (Xu et al., 2010). The simulated SST is consistent with the
374 reconstructions. Although in the early austral summer, over the Indian Ocean warm pool, it is
375 cooler over the SH, while over the Pacific warm pool, it is cooler over the NH (Fig. S7). Such

376 anomalous SST asymmetry may favor the southward shift of the ITCZ over Australia and the
377 southwest Pacific, which might be related to the enhanced austral summer monsoon
378 precipitation. However, the 7MME shows no significant ITCZ shift during the LGM, particularly
379 over the central Australian monsoon region (Fig. S8). The reconstructions and simulations by
380 McGee et al. (2014) and Mohtadi et al. (2014) also suggested that there was no significant shift
381 of ITCZ position during the LGM.

382 Therefore, it is the local dynamical processes, instead of the large-scale circulation such
383 as the position of the ITCZ induced by the NH-SH thermal contrast, that might be the key factor
384 influencing the early summer mean precipitation change over the Australian monsoon region
385 during the LGM. ~~To test this synthesis, we conducted two experiments using a newly developed~~
386 ~~earth system model, the Nanjing University of Information Science and Technology Earth~~
387 ~~System model version 1 (NESM v1, Cao et al., 2015). The PI control run is designed the same as~~
388 ~~PMIP3 protocol. The land sea configuration sensitive run (LSM) is the same as the piControl but~~
389 ~~with the LGM land sea configuration. The two experiments are run 500 years after spin up, and~~
390 ~~the last 100 years are used.~~ To test this hypothesis, we compared the results from the two
391 additional runs, the NESM_PI and the NESM_LSM. The changes of the ND mean precipitation
392 and wind field at 1000 hPa between the NESM_LSM and the NESM_PI ~~piControl~~ are similar to
393 the changes derived from the 7MME, i.e. the precipitation is increased and the convergence is
394 strengthened over northern Australia (Fig. 12a). The changes of the 2-m air temperature, SLP
395 and 850 hPa wind field (Fig. 12b, c) are also similar to those results in the 7MME (Fig. 9). It is
396 also cooler over the northwest landmass (western Indonesia–Indochina) and relatively warmer
397 over the southeast landmass (eastern Indonesia–northern Australia) (Fig. 12b). This temperature
398 variation is also accompanied by a northwest–southeast SLP gradient and the strengthened cross
399 equatorial flow converging to north Australia (Fig. 12c). This ~~sensitive-sensitivity~~ simulation
400 confirms that the local dynamical processes induced by the land sea configuration ~~to be~~
401 essential to the Australian monsoonality change.

402 Although the 7MME simulates strengthened Australian monsoonality, there are
403 uncertainties among individual models. The most notable uncertainty is the increased austral
404 summer (DJF) precipitation. Five out of the 7 models simulate increased DJF mean precipitation
405 over the Australian monsoon region during the LGM (CCSM4, GISS-E2-R, IPSL-CM5A-LR,
406 MIROC-ESM and MRI-CGCM3), while the other two simulate decreased precipitation (CNRM-

407 CM5 and MPI-ESM-P) (Fig. 13), especially over the land area. The wind ~~field~~ at 850hPa
408 geopotential height shows a cyclonic anomaly pattern over northern Australia in the five models
409 (Fig. 14a), accompanied with a strengthened ascending flow (not shown). While in the other two
410 models, there is no cyclonic wind anomaly over Australia region (Fig. 14b), and the ascending
411 flow is weakened (not shown). The different changes of wind field indicate the different
412 precipitation responses to the LGM boundary conditions in the two model groups.

413 The austral spring and summer mean 2m-air temperature and SST also change differently
414 in these two model groups. The main differences are located over the tropic Pacific Ocean and
415 the North Atlantic Ocean. It is cooler over high-latitude Northern Atlantic Ocean in the five
416 models, whereas warmer in the two models, mainly in the austral spring (Fig. 15a, 15b). In the
417 austral summer, there is an ~~East-eastern~~ Pacific El ~~Nino-Nino~~-like patten in the five models,
418 while there is a Central-Pacific El Nino (CP-El Nino) like pattern in the two models (Fig. 15c,
419 15d). Studies have shown that the CP-El Nino is related to the Asian-Australian monsoon system
420 (Yu et al. 2009), and would lead to a markedly decreased precipitation in December (Taschetto
421 et al. 2009).

422 Therefore, the different SST responses over ~~the~~ Pacific Oceans and ~~the~~ North Atlantic
423 Ocean in austral spring and summer in different models might be the key factor that leads to
424 different wind anomalies and thus different Australian monsoon precipitation changes. Note that
425 the resolution of land configuration in each model might not be the key factor that affects the
426 SST gradient over the eastern Indian Ocean and western Pacific Ocean (Fig. S9).

427

428 5 Conclusions

429 The global mean temperature and water vapor have an overall decrease under the LGM
430 forcings (lower GHG and large ice-sheets). Nevertheless, the simulated Australian monsoon
431 seasonality derived from CMIP5/PMIP3 multi-model ensemble has a distinctive amplification
432 (or the monsoonality is intensified) against the weakened global monsoons elsewhere during the
433 LGM. This study then investigated the possible reasons for this strengthened Australian
434 monsoonality from both a thermodynamic and dynamic perspective.

435 The conclusions are as follows:

- 436 1) The Australian monsoon seasonality is strengthened as a result of the enhanced
437 seasonal difference between austral summer and winter, i.e., the increased early
438 summer (ND) mean rainfall and the reduced winter (JJA) mean rainfall. Both the
439 dynamic processes and ~~thermal-thermodynamic~~ effects contribute to the precipitation
440 change; however, the dynamic processes have a much stronger contribution than the
441 ~~thermal-thermodynamic~~ effects.
- 442 2) The Australian winter (JJA mean) precipitation derived from 7MME is decreased
443 during the LGM relative to the preindustrial control experiment. The dynamic
444 processes, induced by the enhanced land–ocean thermal contrast, contribute more to the
445 decreased rainfall through the strengthened divergence over northern Australia (Fig.
446 16a), whereas the thermodynamic effect (i.e., the reduced atmospheric water vapor due
447 to the lower temperature induced by lower GHGs and present ice-sheets) and
448 evaporation have moderate contributions.
- 449 3) For the increased precipitation in early summer (ND) in the 7MME, the local dynamic
450 processes have a positive contribution and the thermodynamic effect has a negative
451 contribution. Both the decomposition method and the ~~sensitive-sensitivity~~ simulations
452 show that the dynamic effect plays most important role for the increased rainfall. The
453 local dynamic processes are mainly induced by the northwest–southeast thermal
454 contrast between Indochina–western Indonesia and northeastern Australia. The east
455 Indian Ocean–west Pacific Ocean thermal gradient also contributes to these processes
456 (Fig. 16b).
- 457 4) The ~~sensitive-sensitivity~~ simulation illustrates that the change in circulation over
458 Australia is very likely to be rooted in the enlarged landmasses over the Indochina–
459 western Indonesia and New Guinea, and northern Australia. Another factor contributes
460 to the circulation change might be the asymmetric change between western Pacific
461 Ocean and eastern Indian Ocean. These have critical impacts on the thermal gradients
462 that induce changes in the low-level circulation pattern and convergence/divergence.

463 Note that models have uncertainties, i.e. not all the models simulate an intensified
464 seasonality of Australian monsoon. The different SST responses over Pacific Ocean and Atlantic
465 Ocean in different models to the same external forcings are essential for the model uncertainties.

466 More model-data comparison and inter-model comparison are required to ~~improve model~~
467 ~~performance~~ better understand the model-data disagreement and improve confidence in model
468 results.

469 Our results are based on the equilibrium simulation, representing a mean state of the
470 Australian monsoon change and its possible mechanisms during the LGM. More simulations
471 with single forcing (such as the SST asymmetry change, the insolation change) are required to
472 further understand the effect of each factor and to specifically quantify the contribution of each
473 forcing to the Australian monsoon change.

474

475 **Acknowledgments**

476 We acknowledge Prof. Williams J and the two reviewers for the comments helping to
477 clarify and improve the paper. This research was jointly supported by the National Key Research
478 and Development Program of China (Grant No. 2016YFA0600401), the National Basic Research
479 Program (Grant No. 2015CB953804), the National Natural Science Foundation of China (Grant
480 Nos. 41671197, 41420104002 and 41501210), and the Priority Academic Development Program
481 of Jiangsu Higher Education Institutions (PAPD, Grant No. 164320H116). We acknowledge the
482 World Climate Research Programme's Working Group on Coupled Modeling, which is
483 responsible for the CMIP, and we thank the climate modeling groups for producing and making
484 available their model outputs. For the CMIP, the U.S. Department of Energy's Program for
485 climate model diagnosis and intercomparison provided coordinating support and led the
486 development of software infrastructure in partnership with the Global Organization for Earth
487 System Science Portals. We thank LetPub (www.letpub.com) for its linguistic assistance during
488 the preparation of this manuscript. This is the ESMC publication XXX.
489

490 **References**

- 491 Ayliffe, L. K., Gagan, M. K., Zhao, J. X., Drysdale, R. N., Hellstrom, J. C., Hantoro, W. S.,
492 Griffiths, M. L., Scott-Gagan, H., St Pierre, E., Cowley, J. A., and Suwargadi, B. W.: Rapid
493 interhemispheric climate links via the Australasian monsoon during the last deglaciation,
494 *Nat Commun*, 4, 2908, 10.1038/ncomms3908, 2013.
- 495 Bayon, G., De Deckker, P., Magee, J. W., Germain, Y., Bermell, S., Tachikawa, K., and
496 Norman, M. D.: Extensive wet episodes in Late Glacial Australia resulting from high-
497 latitude forcings, *Scientific Reports*, 7, 44054, 10.1038/srep44054, 2017.
- 498 Braconnot, P., Otto-Bliesner, B., Harrison, S. P., and al, e.: Results of PMIP2 coupled
499 simulations of the Mid-Holocene and Last Glacial Maximum – Part 2: feedbacks with
500 emphasis on the location of the ITCZ and mid- and high latitudes heat budget, *Climate of*
501 *the Past*, 3, 2007.
- 502 Braconnot, P., Harrison, S. P., Kageyama, M., Bartlein, P. J., Masson-Delmotte, V., Abe-Ouchi,
503 A., Otto-Bliesner, B., and Zhao, Y.: Evaluation of climate models using palaeoclimatic data,
504 *Nature Climate Change*, 2, 417-424, 10.1038/nclimate1456, 2012a.
- 505 Braconnot, P., Harrison, S. P., Otto-Bliesner, B., Abe-Ouchi, A., Jungclaus, J., and Peterschmitt,
506 J. Y.: The Paleoclimate Modeling Intercomparison Project contribution to CMIP5, *CLIVAR*
507 *Exchanges*, 56, 15-19, 2012b.
- 508 Broccoli, A. J., Dahl, K. A., and Stouffer, R. J.: Response of the ITCZ to Northern Hemisphere
509 cooling, *Geophysical Research Letters*, 33(1), L01702, 10.1029/2005gl024546, 2006.
- 510 Brown, J. R., Moise, A. F., Colman, R., and Zhang, H.: Will a Warmer World Mean a Wetter or
511 Drier Australian Monsoon? *Journal of Climate*, 29, 4577-4596, 10.1175/jcli-d-15-0695.1,
512 2016.
- 513 Cao, J., Wang, B., Xiang, B., Li, J., Wu, T., Fu, X., Wu, L., and Min, J.: Major modes of short-
514 term climate variability in the newly developed NUIST Earth System Model (NESM),
515 *Advances in Atmospheric Sciences*, 32, 585-600, 10.1007/s00376-014-4200-6, 2015.
- 516 Chou, C., Neelin, J. D., Chen, C.-A., and Tu, J.-Y.: Evaluating the “Rich-Get-Richer”
517 Mechanism in Tropical Precipitation Change under Global Warming, *Journal of Climate*,
518 22, 1982-2005, 10.1175/2008jcli2471.1, 2009.

519 Cui, X. P.: Quantitative diagnostic analysis of surface rainfall processes by surface rainfall
520 equation. *Chinese Journal of Atmospheric Sciences*, 33(2), 375–387, 2009.

521 De Deckker, P., Barrows, T. T., and Rogers, J.: Land–sea correlations in the Australian region:
522 post-glacial onset of the monsoon in northwestern Western Australia, *Quaternary Science*
523 *Reviews*, 105, 181-194, 10.1016/j.quascirev.2014.09.030, 2014.

524 Denniston, R. F., Wyrwoll, K.-H., Asmerom, Y., Polyak, V. J., Humphreys, W. F., Cugley, J.,
525 Woods, D., LaPointe, Z., Peota, J., and Greaves, E.: North Atlantic forcing of millennial-
526 scale Indo-Australian monsoon dynamics during the Last Glacial period, *Quaternary*
527 *Science Reviews*, 72, 159-168, 10.1016/j.quascirev.2013.04.012, 2013.

528 Denniston, R. F., Asmerom, Y., Polyak, V. J., Wanamaker, A. D., Ummenhofer, C. C.,
529 Humphreys, W. F., Cugley, J., Woods, D., and Lucker, S.: Decoupling of monsoon activity
530 across the northern and southern Indo-Pacific during the Late Glacial, *Quaternary Science*
531 *Reviews*, 176, 101-105, 10.1016/j.quascirev.2017.09.014, 2017.

532 DiNezio, P. N., Timmermann, A., Tierney, J. E., Jin, F.-F., Otto-Bliesner, B., Rosenbloom, N.,
533 Mapes, B., Neale, R., Ivanovic, R. F., and Montenegro, A.: The climate response of the
534 Indo-Pacific warm pool to glacial sea level, *Paleoceanography*, 31, 866-894,
535 10.1002/2015PA002890, 2016.

536 DiNezio, P. N., Clement, A., Vecchi, G. A., Soden, B., Broccoli, A. J., Otto-Bliesner, B. L., and
537 Braconnot, P.: The response of the Walker circulation to Last Glacial Maximum forcing:
538 Implications for detection in proxies, *Paleoceanography*, 26, n/a-n/a,
539 10.1029/2010pa002083, 2011.

540 DiNezio, P. N., and Tierney, J. E.: The effect of sea level on glacial Indo-Pacific climate, *Nature*
541 *Geoscience*, 6, 485-491, 10.1038/ngeo1823, 2013.

542 Donohoe, A., Marshall, J., Ferreira, D., and McGee, D.: The Relationship between ITCZ
543 Location and Cross-Equatorial Atmospheric Heat Transport: From the Seasonal Cycle to
544 the Last Glacial Maximum, *Journal of Climate*, 26, 3597-3618, 10.1175/jcli-d-12-00467.1,
545 2013.

546 Endo, H., and Kitoh, A.: Thermodynamic and dynamic effects on regional monsoon rainfall
547 changes in a warmer climate, *Geophysical Research Letters*, 41, 1704-1711,
548 10.1002/2013gl059158, 2014.

549 Eroglu, D., McRobie, F. H., Ozken, I., Stemler, T., Wyrwoll, K. H., Breitenbach, S. F., Marwan,
550 N., and Kurths, J.: See-saw relationship of the Holocene East Asian-Australian summer
551 monsoon, *Nat Commun*, 7, 12929, 10.1038/ncomms12929, 2016.

552 Hargreaves, J. C., Annan, J. D., Ohgaito, R., Paul, A., and Abe-Ouchi, A.: Skill and reliability of
553 climate model ensembles at the Last Glacial Maximum and mid-Holocene, *Climate of the*
554 *Past*, 9, 811-823, 10.5194/cp-9-811-2013, 2013.

555 Harrison, S. P., Bartlein, P. J., Brewer, S., Prentice, I. C., Boyd, M., Hessler, I., Holmgren, K.,
556 Izumi, K., and Willis, K.: Climate model benchmarking with glacial and mid-Holocene
557 climates, *Climate Dynamics*, 43, 671-688, 10.1007/s00382-013-1922-6, 2014.

558 Held, I. M., and Soden, B. J.: Robust responses of the hydrological cycle to global warming,
559 *Journal of Climate*, 19, 5686-5699, 2006.

560 Hewitt, C., Broccoli, A. J., Mitchell, J. F. B., and Stouffer, R.: A coupled model study of the last
561 glacial maximum: Was part of the North Atlantic relatively warm? *Geophys. Res. Lett.*, 28,
562 1571-1574, 2001.

563 Huang, P., Xie, S.-P., Hu, K., Huang, G., and Huang, R.: Patterns of the seasonal response of
564 tropical rainfall to global warming, *Nature Geoscience*, 6, 357-361, 10.1038/ngeo1792,
565 2013.

566 Huffman, G. J., Adler, R. F., Bolvin, D. T., and Gu, G.: Improving the global precipitation
567 record: GPCP Version 2.1, *Geophysical Research Letters*, 36, 10.1029/2009gl040000, 2009.

568 Jiang, D., Tian, Z., Lang, X., Kageyama, M., and Ramstein, G.: The concept of global monsoon
569 applied to the last glacial maximum: A multi-model analysis, *Quaternary Science Reviews*,
570 126, 126-139, 10.1016/j.quascirev.2015.08.033, 2015.

571 Jourdain, N. C., Gupta, A. S., Taschetto, A. S., Ummenhofer, C. C., Moise, A. F., and Ashok, K.:
572 The Indo-Australian monsoon and its relationship to ENSO and IOD in reanalysis data and
573 the CMIP3/CMIP5 simulations, *Climate Dynamics*, 41, 3073-3102, 10.1007/s00382-013-
574 1676-1, 2013.

575 Kuhnt, W., Holbourn, A., Xu, J., Opdyke, B., De Deckker, P., Rohl, U., and Mudelsee, M.:
576 Southern Hemisphere control on Australian monsoon variability during the late deglaciation
577 and Holocene, *Nat Commun*, 6, 5916, 10.1038/ncomms6916, 2015.

578 Li, J., Feng, J., and Li, Y.: A possible cause of decreasing summer rainfall in northeast Australia,
579 *International Journal of Climatology*, 32, 995-1005, 10.1002/joc.2328, 2012.

580 Liu, F., Chai, J., Wang, B., Liu, J., Zhang, X., and Wang, Z.: Global monsoon precipitation
581 responses to large volcanic eruptions, *Sci Rep*, 6, 24331, 10.1038/srep24331, 2016.

582 Liu, Y., Lo, L., Shi, Z., Wei, K. Y., Chou, C. J., Chen, Y. C., Chuang, C. K., Wu, C. C., Mii, H.
583 S., Peng, Z., Amakawa, H., Burr, G. S., Lee, S. Y., DeLong, K. L., Elderfield, H., and Shen,
584 C. C.: Obliquity pacing of the western Pacific Intertropical Convergence Zone over the past
585 282,000 years, *Nat Commun*, 6, 10018, 10.1038/ncomms10018, 2015.

586 Marshall, A. G., and Lynch, A. H.: Time-slice analysis of the Australian summer monsoon
587 during the late Quaternary using the Fast Ocean Atmosphere Model, *Journal of Quaternary
588 Science*, 21, 789-801, 10.1002/jqs.1063, 2006.

589 Marshall, A. G., and Lynch, A. H.: The sensitivity of the Australian summer monsoon to climate
590 forcing during the late Quaternary, *Journal of Geophysical Research*, 113,
591 10.1029/2007jd008981, 2008.

592 McGee, D., Donohoe, A., Marshall, J., and Ferreira, D.: Changes in ITCZ location and cross-
593 equatorial heat transport at the Last Glacial Maximum, Heinrich Stadial 1, and the mid-
594 Holocene, *Earth and Planetary Science Letters*, 390, 69-79, 10.1016/j.epsl.2013.12.043,
595 2014.

596 Miller, G. H., Fogel, M. L., Magee, J. W., and Gagan, M. K.: Disentangling the impacts of
597 climate and human colonization on the flora and fauna of the Australian arid zone over the
598 past 100 ka using stable isotopes in avian eggshell, *Quaternary Science Reviews*, 151, 27-
599 57, 10.1016/j.quascirev.2016.08.009, 2016.

600 Mohtadi, M., Prange, M., Oppo, D. W., De Pol-Holz, R., Merkel, U., Zhang, X., Steinke, S., and
601 Lückge, A.: North Atlantic forcing of tropical Indian Ocean climate, *Nature*, 509, 76,
602 10.1038/nature13196, 2014.

603 Petherick, L., Bostock, H., Cohen, T. J., Fitzsimmons, K., Tibby, J., Fletcher, M. S., Moss, P.,
604 Reeves, J., Mooney, S., Barrows, T., Kemp, J., Jansen, J., Nanson, G., and Dosseto, A.:
605 Climatic records over the past 30 ka from temperate Australia – a synthesis from the Oz-
606 INTIMATE workgroup, *Quaternary Science Reviews*, 74, 58-77,
607 10.1016/j.quascirev.2012.12.012, 2013.

608 Reeves, J. M., Barrows, T. T., Cohen, T. J., Kiem, A. S., Bostock, H. C., Fitzsimmons, K. E.,
609 Jansen, J. D., Kemp, J., Krause, C., Petherick, L., and Phipps, S. J.: Climate variability over
610 the last 35,000 years recorded in marine and terrestrial archives in the Australian region: an
611 OZ-INTIMATE compilation, *Quaternary Science Reviews*, 74, 21-34,
612 10.1016/j.quascirev.2013.01.001, 2013a.

613 Reeves, J. M., Bostock, H. C., Ayliffe, L. K., Barrows, T. T., De Deckker, P., Devriendt, L. S.,
614 Dunbar, G. B., Drysdale, R. N., Fitzsimmons, K. E., Gagan, M. K., Griffiths, M. L.,
615 Haberle, S. G., Jansen, J. D., Krause, C., Lewis, S., McGregor, H. V., Mooney, S. D., Moss,
616 P., Nanson, G. C., Purcell, A., and van der Kaars, S.: Palaeoenvironmental change in
617 tropical Australasia over the last 30,000 years – a synthesis by the OZ-INTIMATE group,
618 *Quaternary Science Reviews*, 74, 97-114, 10.1016/j.quascirev.2012.11.027, 2013b.

619 Rojas, M.: Sensitivity of Southern Hemisphere circulation to LGM and $4 \times \text{CO}_2$ climates,
620 *Geophysical Research Letters*, 40, 965-970, 10.1002/grl.50195, 2013.

621 Seager, R., Naik, N., and Vecchi, G. A.: Thermodynamic and Dynamic Mechanisms for Large-
622 Scale Changes in the Hydrological Cycle in Response to Global Warming*, *Journal of*
623 *Climate*, 23, 4651-4668, 10.1175/2010jcli3655.1, 2010.

624 Taylor, K. E., Stouffer, R. J., and Meehl, G. A.: An Overview of CMIP5 and the Experiment
625 Design, *Bulletin of the American Meteorological Society*, 93, 485-498, 10.1175/bams-d-11-
626 00094.1, 2012.

627 Tharammal, T., Paul, A., Merkel, U., and Noone, D.: Influence of Last Glacial Maximum
628 boundary conditions on the global water isotope distribution in an atmospheric general
629 circulation model, *Climate of the Past*, 9, 789-809, 10.5194/cp-9-789-2013, 2013.

630 Turney, C. S. M., Haberle, S., Fink, D., Kershaw, A. P., Barbetti, M., Barrows, T. T., Black, M.,
631 Cohen, T. J., Corrège, T., Hesse, P. P., Hua, Q., Johnston, R., Morgan, V., Moss, P.,

632 Nanson, G., van Ommen, T., Rule, S., Williams, N. J., Zhao, J. X., D'Costa, D., Feng, Y.
633 X., Gagan, M., Mooney, S., and Xia, Q.: Integration of ice-core, marine and terrestrial
634 records for the Australian Last Glacial Maximum and Termination: a contribution from the
635 OZ INTIMATE group, *Journal of Quaternary Science*, 21, 751-761, 10.1002/jqs.1073,
636 2006.

637 Wang, B., and Ding, Q.: Global monsoon: Dominant mode of annual variation in the tropics,
638 *Dynamics of Atmospheres and Oceans*, 44, 165-183, 10.1016/j.dynatmoce.2007.05.002,
639 2008.

640 Wang, P. X., Wang, B., Cheng, H., Fasullo, J., Guo, Z., Kiefer, T., and Liu, Z.: The global
641 monsoon across time scales: Mechanisms and outstanding issues, *Earth-Science Reviews*,
642 10.1016/j.earscirev.2017.07.006, 2017.

643 Williams, A. N., Ulm, S., Cook, A. R., Langley, M. C., and Collard, M.: Human refugia in
644 Australia during the Last Glacial Maximum and Terminal Pleistocene: a geospatial analysis
645 of the 25–12 ka Australian archaeological record, *Journal of Archaeological Science*, 40,
646 4612-4625, 10.1016/j.jas.2013.06.015, 2013.

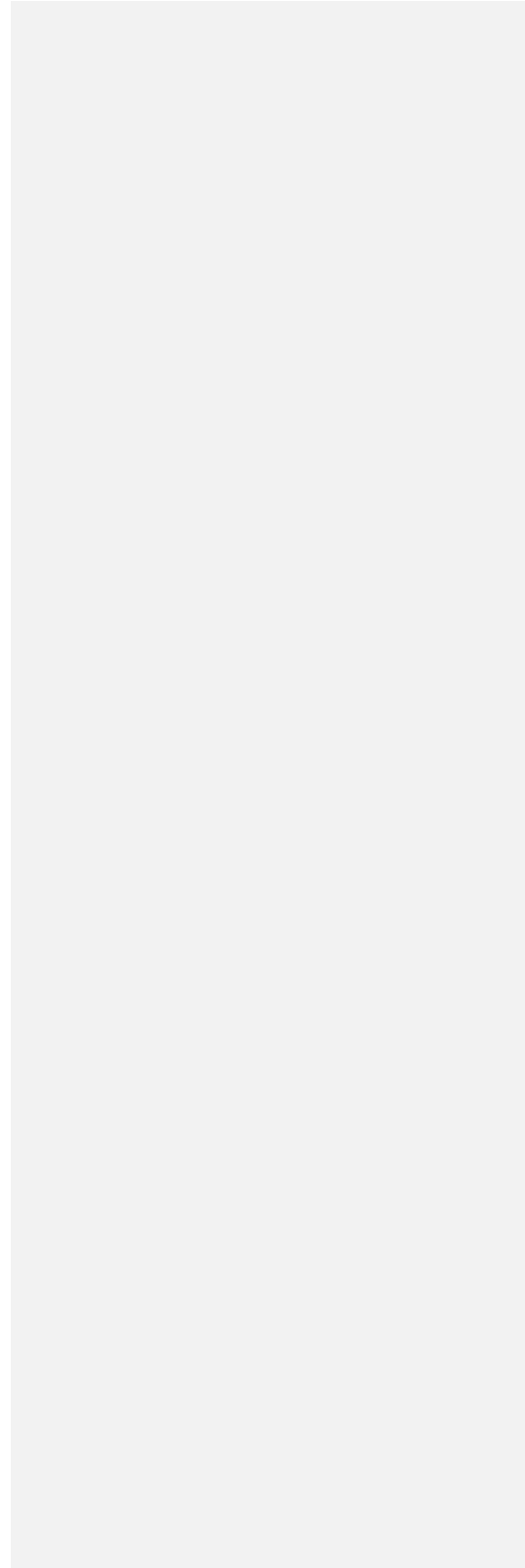
647 Wyrwoll, K.-H., Liu, Z., Chen, G., Kutzbach, J. E., and Liu, X.: Sensitivity of the Australian
648 summer monsoon to tilt and precession forcing, *Quaternary Science Reviews*, 26, 3043-
649 3057, 10.1016/j.quascirev.2007.06.026, 2007.

650 Wyrwoll, K.-H., Hopwood, J. M., and Chen, G.: Orbital time-scale circulation controls of the
651 Australian summer monsoon: a possible role for mid-latitude Southern Hemisphere forcing?
652 *Quaternary Science Reviews*, 35, 23-28, 10.1016/j.quascirev.2012.01.003, 2012.

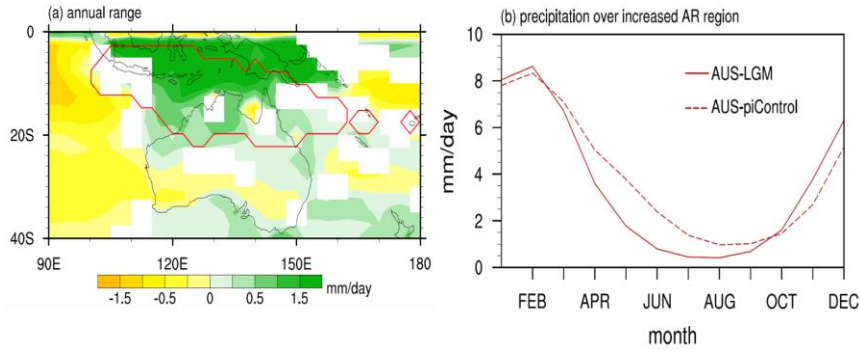
653 Xie, P., and Arkin, P.: Global precipitation: a 17-year monthly analysis based on Gauge
654 Observations, satellite estimates, and numerical model outputs, *Bulletin of the American
655 Meteorological Society*, 78, 2539-2558, 1997.

656 Xu, J., Kuhnt, W., Holbourn, A., Regenberg, M., and Andersen, N.: Indo-Pacific Warm Pool
657 variability during the Holocene and Last Glacial Maximum, *Paleoceanography*, 25,
658 10.1029/2010pa001934, 2010.

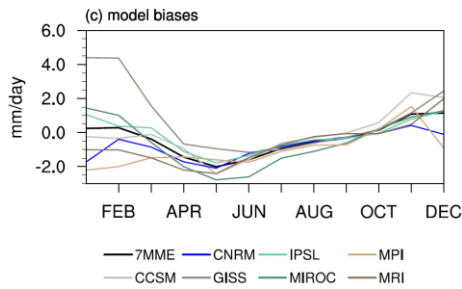
659 Yan, M., Wang, B., and Liu, J.: Global monsoon change during the Last Glacial Maximum: a
660 multi-model study, *Climate Dynamics*, 47, 359-374, 10.1007/s00382-015-2841-5, 2016.



662



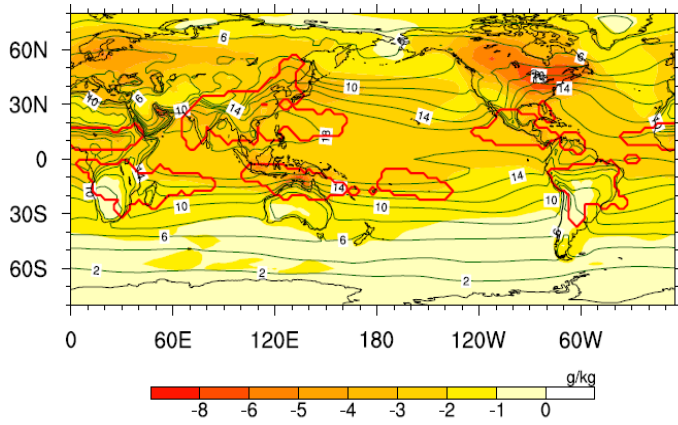
663



664

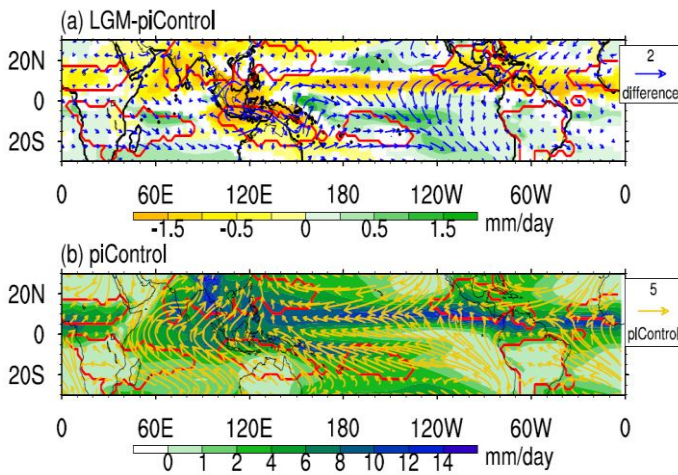
665 **Figure 1** (a) Spatial distribution of changes in the annual range (AR) of precipitation measured
666 by the difference between LGME and piControl, (b) seasonal distribution of the precipitation in
667 the increased AR area (20°S-5°S, 120°E-145°E), and (c) seasonal distribution of the precipitation
668 differences in the increased AR area derived from 7 MME (black line) and each model (colored
669 lines). The red solid line in (a) encloses the Australian monsoon rainfall domain. The dashed
670 (solid) line in (b) denotes the seasonal distribution of precipitation derived from the piControl
671 (LGME) run. Only those areas where signal-to-noise ratio exceeds one are plotted in (a).

672



673
 674 **Figure 2** Difference of JJA mean surface specific humidity between LGME and piControl
 675 (shaded). The green contours denote the climatology derived from piControl. The red lines
 676 enclose the monsoon domains. Only those areas where signal-to-noise ratio exceeds one are
 677 plotted.

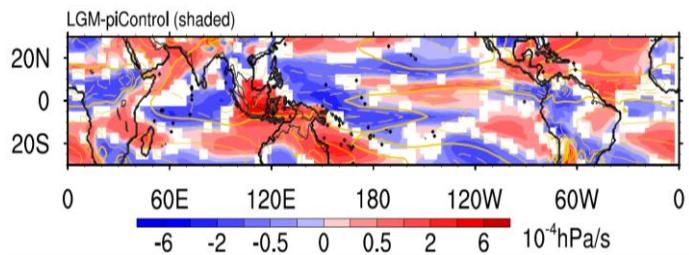
678



679
 680 **Figure 3** (a) JJA mean precipitation (shading) difference and surface wind (vectors) difference
 681 between LGME and piControl, and (b) the climatology of JJA mean precipitation (shading) and
 682 surface wind (vectors) derived from piControl. The red lines enclose the monsoon domains. The
 683 thick black lines in (a) denote the coastal lines in LGME [provided by CMIP5/PMIP3](#), and the

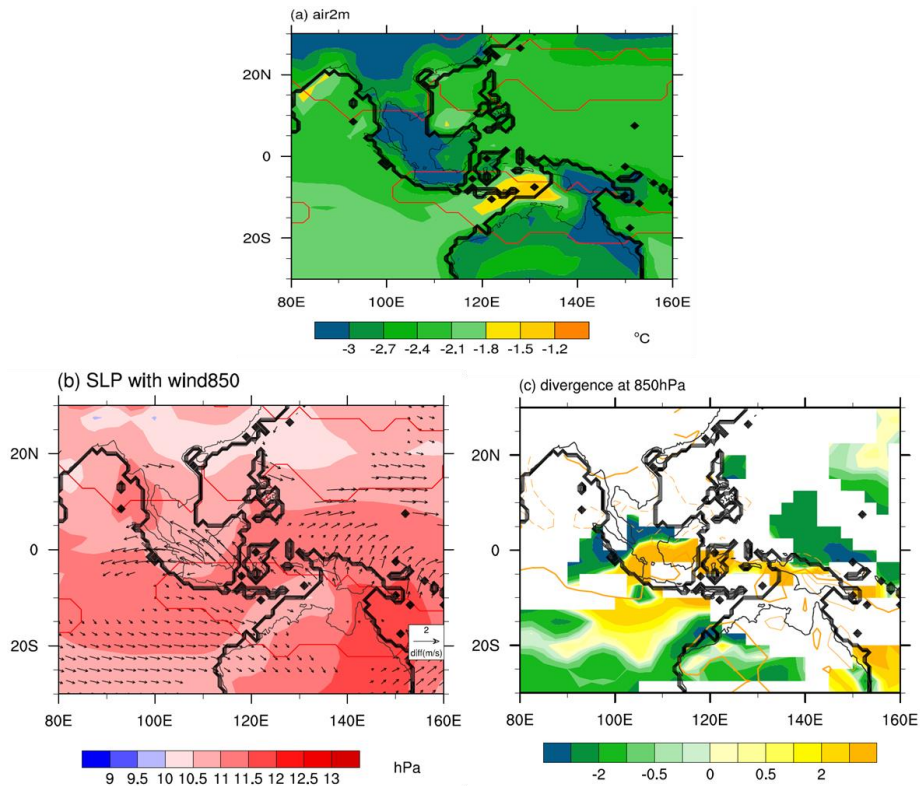
684 thin black lines denote the coastal lines in piControl. Only those areas where signal-to-noise ratio
685 exceeds one are plotted in (a).

686



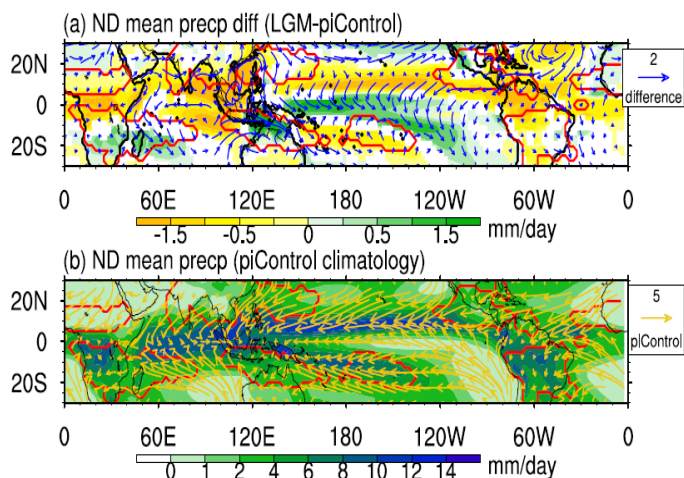
687 **Figure 4** The difference of JJA mean vertical velocity at 500 hPa between LGME and piControl
688 (in shading) and the corresponding climatology derived from piControl (yellow contours). The
689 thick black lines denote the coastal lines in LGME [provided by CMIP5/PMIP3](#), and the thin
690 black lines denote the coastal lines in piControl. Only those areas where signal-to-noise ratio
691 exceeds one are plotted in the difference pattern.

693

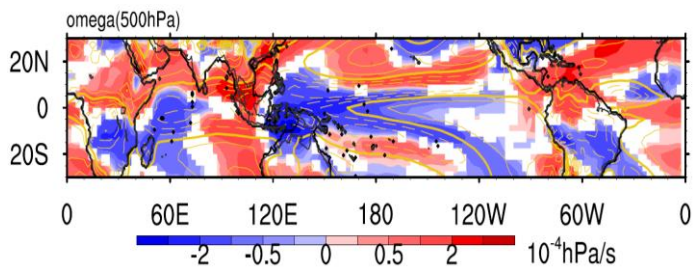


694
 695 **Figure 5** JJA mean (a) surface air temperature, (b) sea level pressure (shading) with 850 hPa
 696 wind (vector), and (c) 850 hPa divergence differences between LGME and piControl. The red
 697 lines in (a) and (b) enclose the monsoon domains. The orange lines in (c) represent the
 698 climatology derived from piControl. The thick black lines denote the coastal lines in LGME
 699 [provided by CMIP5/PMIP3](#), and the thin black lines denote the coastal lines in piControl. Only
 700 those areas where signal-to-noise ratio exceeds one are plotted.

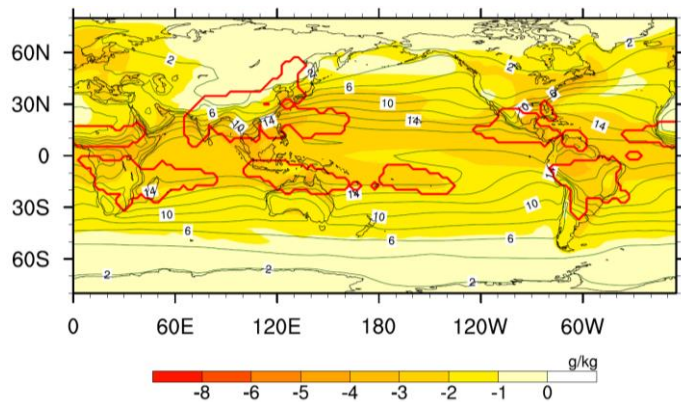
701



702
 703 **Figure 6** (a) ND mean precipitation (shading) difference and surface wind (vectors) difference
 704 between LGME and piControl, and (b) the climatology of ND mean precipitation (shading) and
 705 surface wind (vectors) derived from piControl. The red lines enclose the monsoon domains. The
 706 thick black lines in (a) denote the coastal lines in LGME [provided by CMIP5/PMIP3](#), and the
 707 thin black lines denote the coastal lines in piControl. Only those areas where signal-to-noise ratio
 708 exceeds one are plotted in (a).
 709

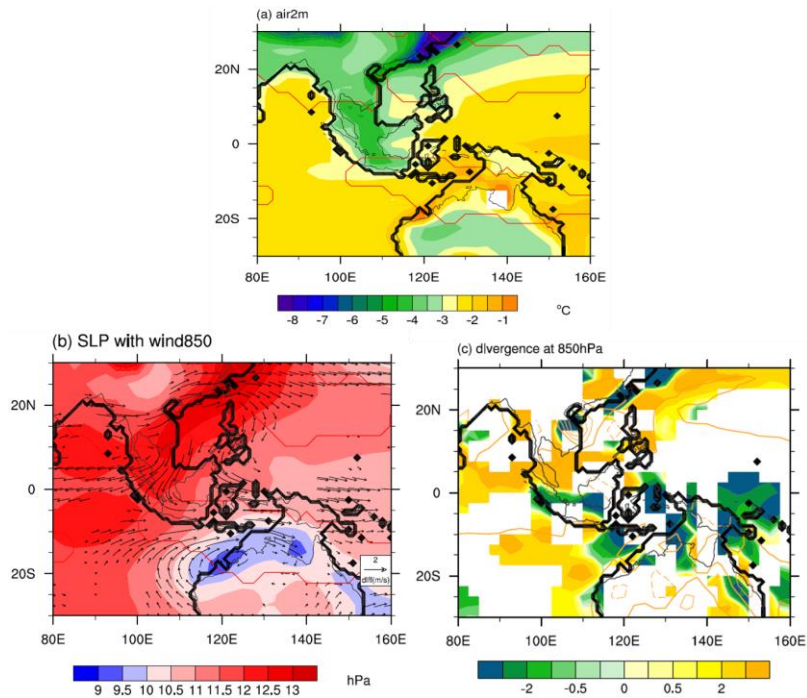


710
 711 **Figure 7** The difference of the ND mean vertical velocity at 500 hPa between LGME and
 712 piControl (in shading) and the corresponding climatology derived from piControl (yellow
 713 contours). The thick black lines denote the coastal lines in LGME [provided by CMIP5/PMIP3](#),
 714 and the thin black lines denote the coastal lines in piControl. Only those areas where signal-to-
 715 noise ratio exceeds one are plotted in the difference pattern.
 716



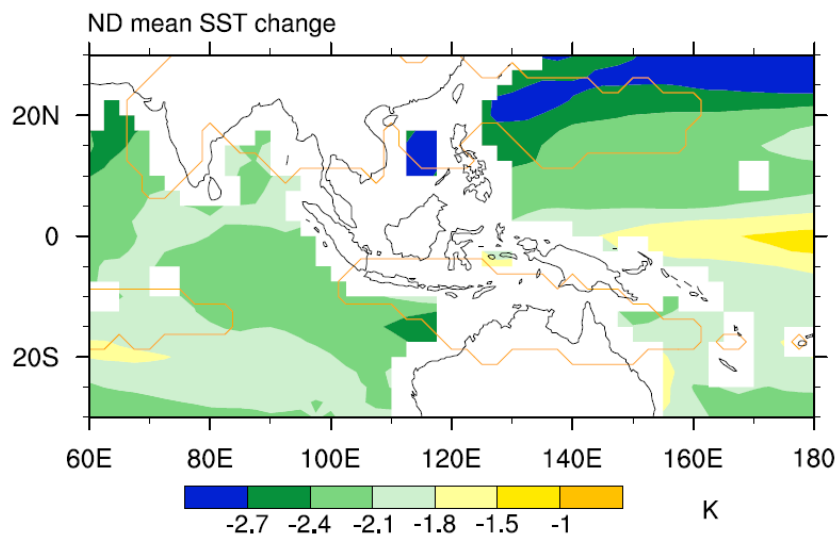
717
 718 **Figure 8** Difference of ND mean surface specific humidity between LGME and piControl
 719 (shaded). The green contours denote the climatology derived from piControl. The red lines
 720 enclose the monsoon domains. Only those areas where signal-to-noise ratio exceeds one are
 721 plotted.

722



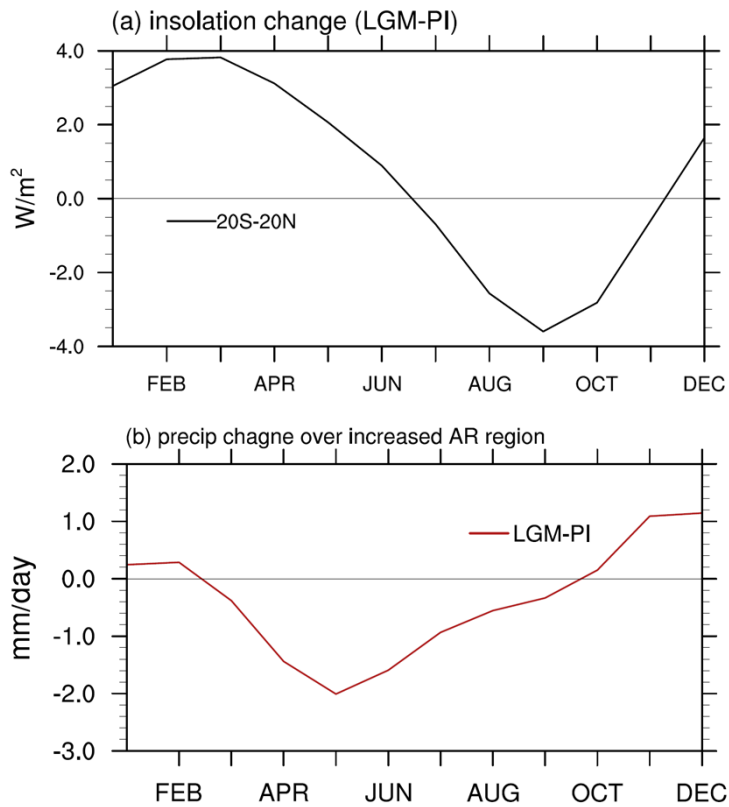
723
 724 **Figure 9** ND mean **(a)** surface air temperature, **(b)** sea level pressure (shading) with 850 hPa
 725 wind (vector), and **(c)** 850 hPa divergence difference between LGME and piControl (shading).
 726 The red lines in **(a)** and **(b)** enclose the monsoon domains. The orange lines in **(c)** represents the
 727 climatology derived from piControl. The thick black lines denote the coastal lines in LGME
 728 [provided by CMIP5/PMIP3](#), and the thin black lines denote the coastal lines in piControl. Only
 729 those areas where signal-to-noise ratio exceeds one are plotted.

730



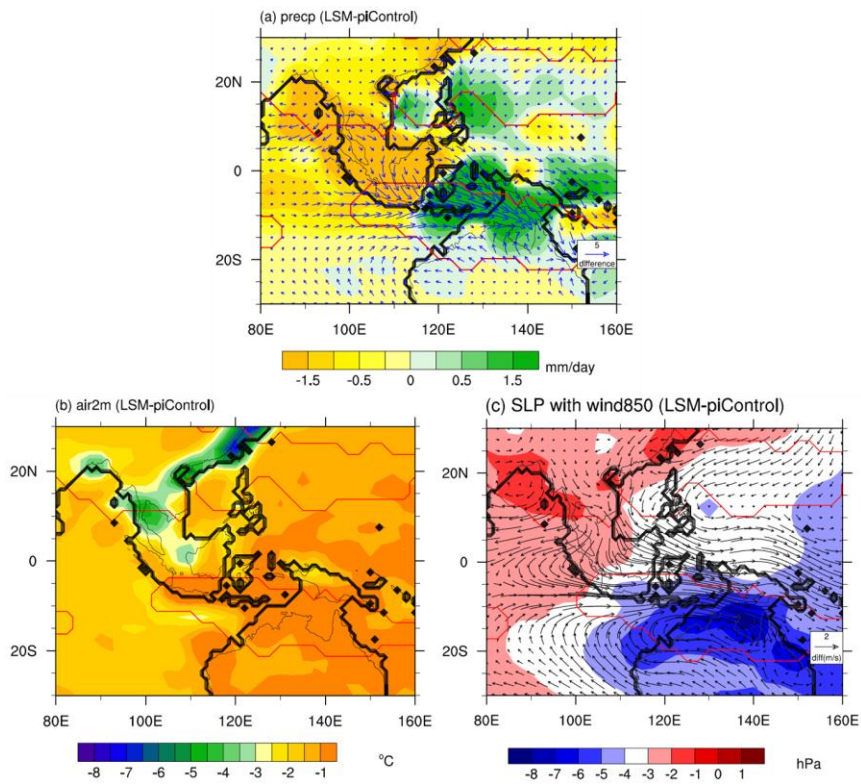
731
732 **Figure 10** ND mean SST difference between LGME and piControl. The red lines enclose the
733 monsoon domains. Only those areas where signal-to-noise ratio exceeds one are plotted.

734

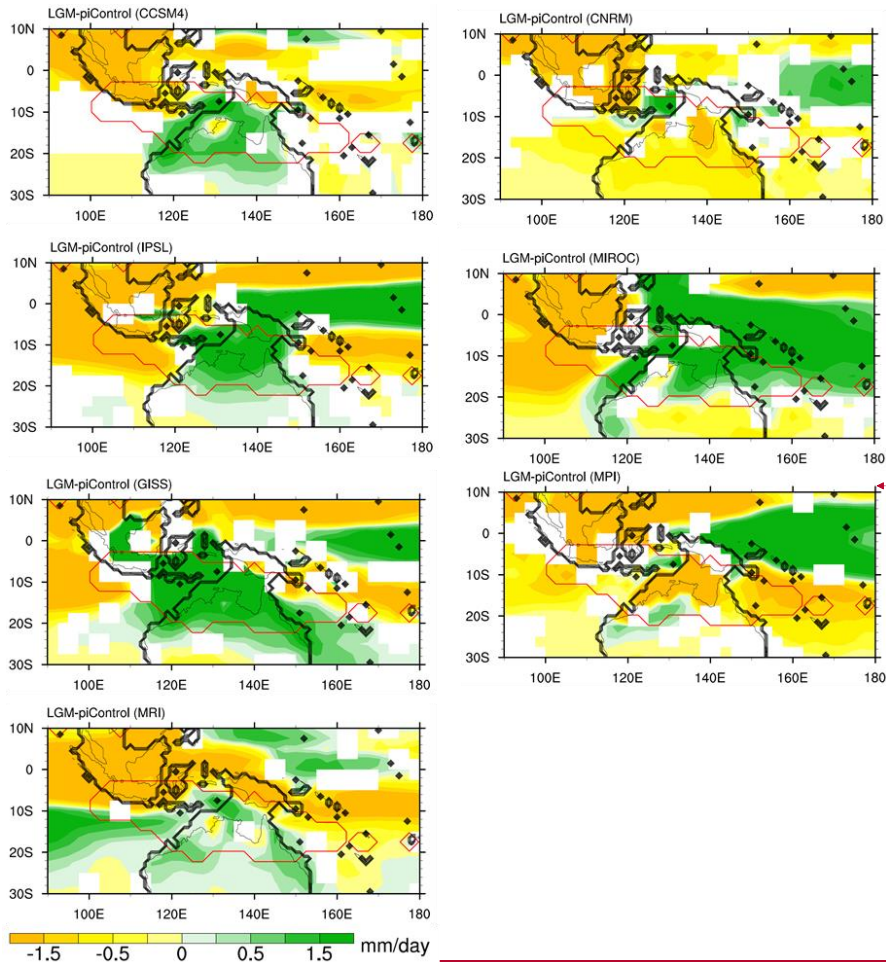


735
 736 **Figure 11** Seasonal distribution of (a) insolation change between 20 °S and 20 °N, and (b)
 737 precipitation change over the increased AR region as indicated in Fig. 1b (20 °S-5 °S, 120 °E-
 738 145 °E). The changes are calculated by the LGM value minus the PI value.

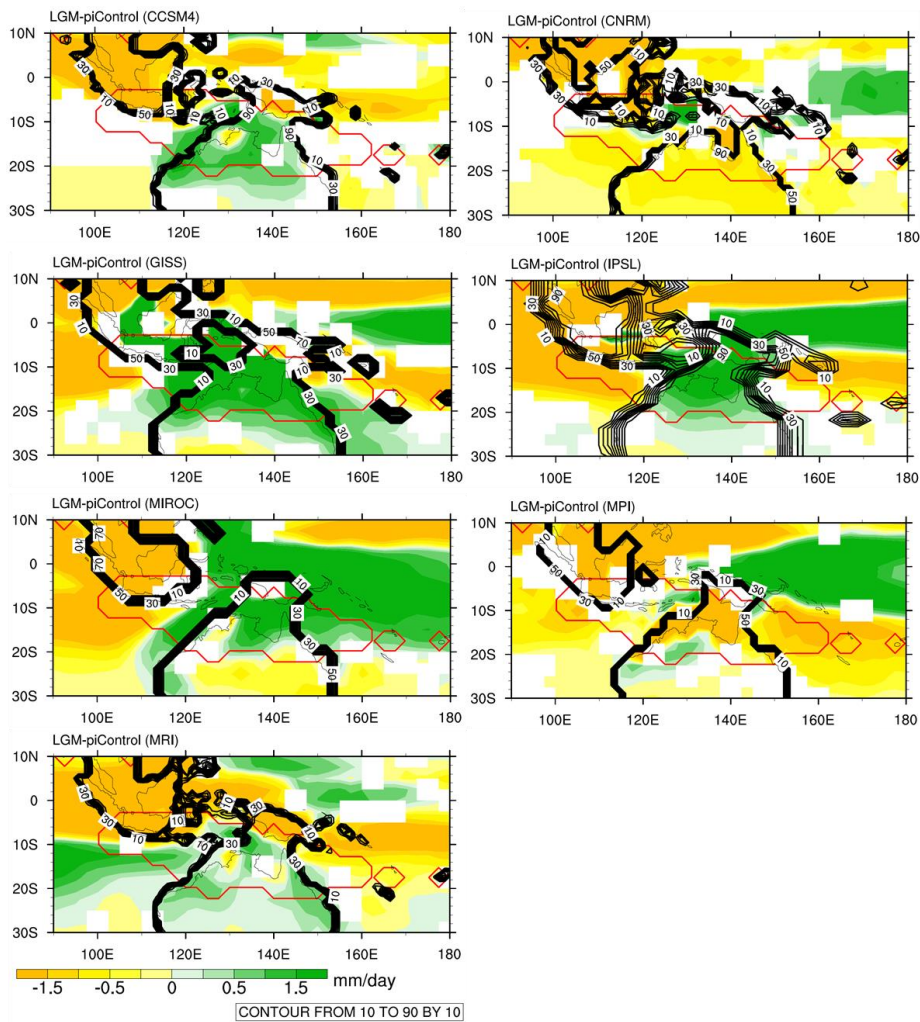
739
 740
 741
 742
 743
 744
 745



746
 747 **Figure 12** ND mean (a) precipitation (shading) with 1000 hPa wind (vector), (b) surface air
 748 temperature, and (c) sea level pressure (shading) with 850 hPa wind (vector) difference between
 749 the NESM LSM and the NESM PI and sea configuration experiment (LSM) and piControl. The
 750 red lines enclose the monsoon domains. The thick black lines denote the coastal lines in
 751 NESM_LSM, and the thin black lines denote the coastal lines in piControl/NESM_PI.



带格式的: 居中



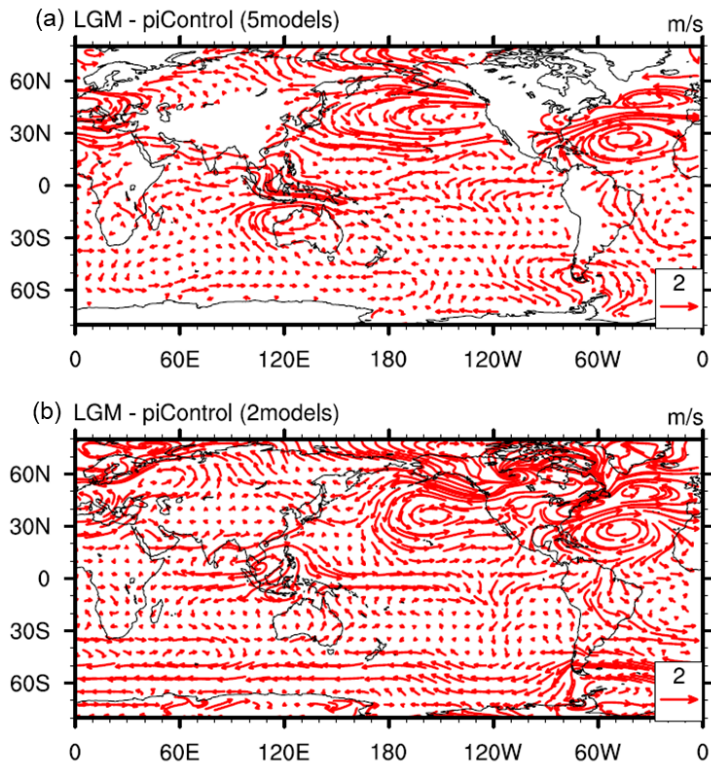
753
 754 **Figure 13** DJF mean precipitation differences between LGME and piControl derived from each
 755 model. The red lines enclose the monsoon domains. The dark black lines show the land area
 756 fraction used for the LGME in each model. Only those areas where signal-to-noise ratio exceeds
 757 one are plotted.

758

759

760

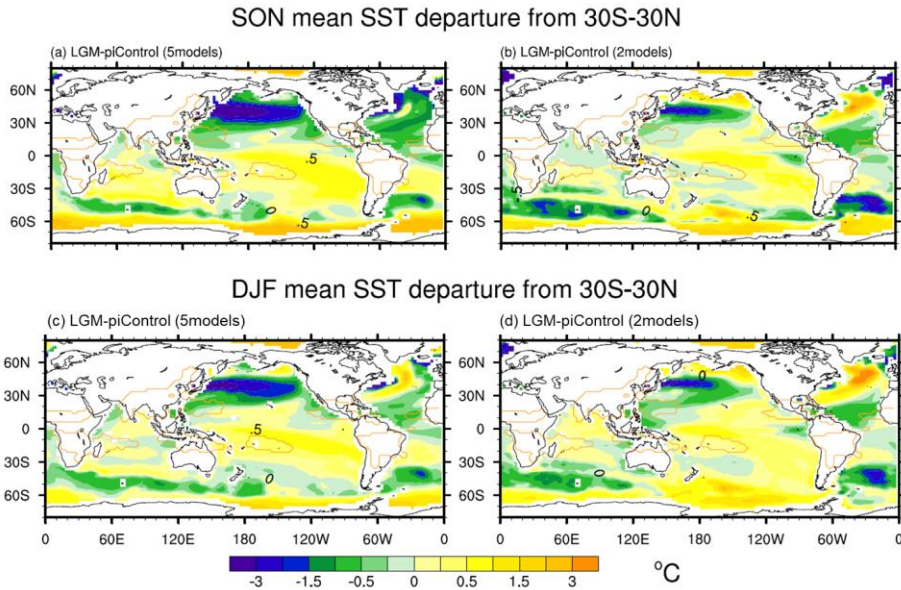
761



762

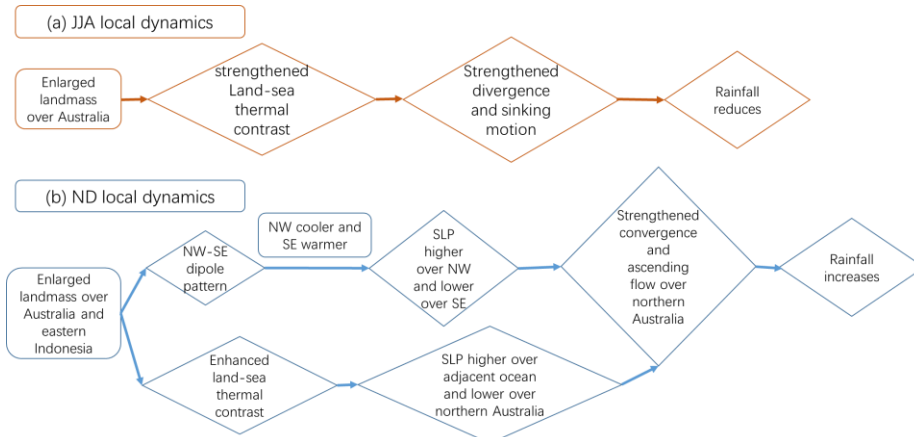
763 **Figure 14** DJF mean 850hPa wind differences between LGME and piControl derived from (a)
764 the five models and (b) the two models. Only those areas where signal-to-noise ratio exceeds one
765 are plotted.

766



767
 768 **Figure 15** SON mean (a)-(b) and DJF mean (c)-(d) SST differences between LGME and
 769 piControl derived from (a), (c) the five models and (b), (d) the two models. Only those areas
 770 where signal-to-noise ratio exceeds one are plotted. The area average of tropical (30 °S-30 °N)
 771 SST change is distracted to make it clearer to illustrate the regional differences.

772
 773



774

775 **Figure 12** Mechanisms of Australian monsoon precipitation change **(a)** in JJA, and **(b)** in ND
776 during the LGM, in the local dynamics perspective.

777

778

779

780 **Table 1** CMIP5/PMIP3 models and experiments used in this study.

| Model | Institution | piControl Time span (years) | LGME Time span (years) | Spatial resolution for atmospheric module Lon × Lat Grids | Spatial resolution for oceanic module Lon × Lat Grids |
|--------------------------|--|--|---|--|--|
| CCSM4 | National Centre for Atmospheric Research (NCAR) | 501 | 101 | 288 × 192 | 320×384 |
| CNRM- CM5 | Centre National de Recherches Meteorologiques/Centre Europeen de Recherche et Formation Avancees en Calcul Scientifique (CNRM-CERFACS) | 850 | 200 | 256 × 128 | 362×292 |
| GISS-E2-R | NASA Goddard Institute for Space Studies (NASA GISS) | 1200 | 100 | 144 × 90 | 288×180 |
| IPSL- CM5A-LR | Institute Pierre-Simon Laplace (IPSL) | 1000 | 200 | 96 × 95 | 182×149 |
| MIROC- ESM | Atmosphere and Ocean Research Institute, University of Tokyo, National Institute for Environmental studies, and Japan Agency for Marine-Earth Science and Technology | 531 | 100 | 128 × 64 | 256×192 |
| MPI-ESM- P | Max Planck Institute for Meteorology | 1156 | 100 | 196 × 98 | 256×220 |
| MRI- CGCM3 | Meteorological Research Institute (MRI) | 500 | 100 | 320 × 160 | 364×368 |

781
782
783

Table 2 Main changed boundary conditions used for the piControl and LGME experiments.

| | piControl | LGME |
|---------------------------|--|--|
| Orbital parameters | Eccentricity = 0.016724 Obliquity = 23.446° Angular precession = 102.04° | Eccentricity = 0.018994 Obliquity = 22.949° Angular precession = 114.42° |
| Trace gases | CO ₂ = 280 ppm CH ₄ = 650 ppb N ₂ O = 270 ppb | CO ₂ = 185 ppm CH ₄ = 350 ppb N ₂ O = 200 ppb |
| Ice sheets | Modern | Provided by ICE-6G v2 (Peltier, 2009) |

Land surface elevation Modern Provided by PMIP3

and coastlines

784

785 Table 3 Annual mean, austral summer (DJF) mean and annual range of precipitation change over
 786 the region of (20 °S-5 °S, 120 °E-145 °E). The area averaged value is calculated based on the
 787 areas where S2N ratio exceed one.

| Model | Annual mean (mm/day) | Summer mean (mm/day) | Annual range (mm/day) |
|---------------------|---------------------------------|---------------------------------|----------------------------------|
| CCSM4 | -0.14 | 0.49 | 1.36 |
| CNRM-CM5 | -0.78 | -0.74 | 0.12 |
| GISS-E2-R | 0.79 | 3.74 | 4.66 |
| IPSL-CM5A-LR | -0.17 | 0.90 | 1.82 |
| MIROC-ESM | -0.53 | 1.25 | 3.17 |
| MPI-ESM-P | -1.02 | -1.71 | -0.52 |
| MRI-CGCM3 | -0.68 | -0.01 | 0.85 |
| 7MME | -0.36 | 0.56 | 1.61 |

788

1 Supporting Information for

2 **Understanding the Australian Monsoon change during the**
3 **Last Glacial Maximum with multi-model ensemble**

4 **Mi Yan^{1,2}, Bin Wang^{3,4}, Jian Liu^{1,2*}, Axing Zhu^{1,2,5,6}, Liang Ning^{1,2,7}, Jian Cao⁴**

5 1 Key Laboratory of Virtual Geographic Environment, Ministry of Education; State key
6 Laboratory of Geographical Environment Evolution, Jiangsu Provincial Cultivation Base;
7 School of Geography Science, Nanjing Normal University, Nanjing, 210023, China.

8 2 Jiangsu Center for Collaborative Innovation in Geographical Information Resource
9 Development and Application, Nanjing, 210023, China.

10 3 Department of Atmospheric Sciences, University of Hawaii at Manoa, Honolulu, HI
11 96825, USA.

12 4 Earth System Modeling Center, Nanjing University of Information Science and
13 Technology, Nanjing, 210044, China.

14 5 State Key Lab of Resources and Environmental Information System, Institute of
15 Geographic Sciences and Natural Resources Research, Chinese Academy of Sciences,
16 Beijing, 100101, China

17 6 Department of Geography, University of Wisconsin-Madison, Madison, WI 53706,
18 USA

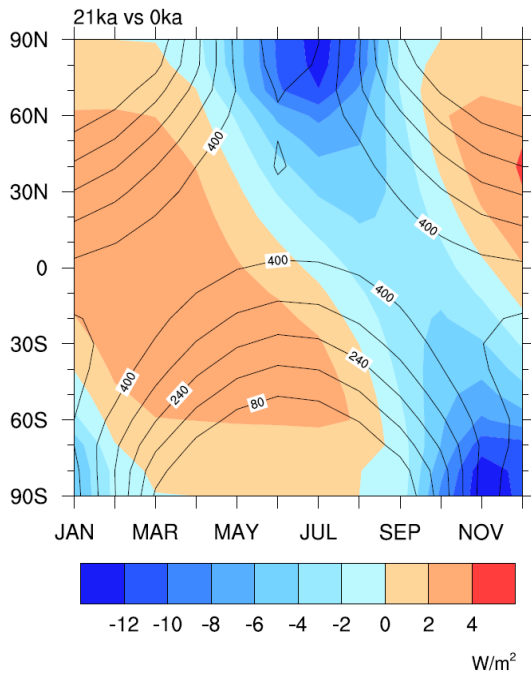
19 7 Climate System Research Center, Department of Geosciences, University of
20 Massachusetts, Amherst, 01003, USA.

21
22 * Corresponding author address: Dr. Jian Liu, School of Geography Science, Nanjing
23 Normal University, 1 Wenyuan Road, Nanjing 210023, China

24 E-mail: jliu@njnu.edu.cn

25

26
27



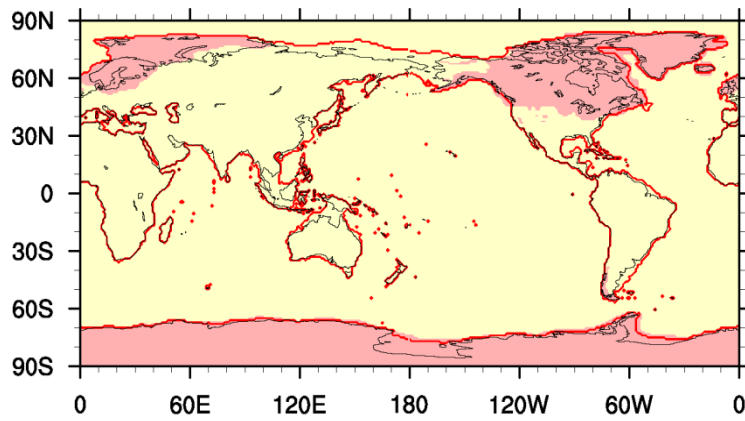
28

29 **Figure S1** Change of the insolation during the LGM. The insolation during PI is plotted in
30 contours, and the difference between the LGM and the PI is color-shaded (units in W m⁻²).

31 [Reprint of Fig. 2 in Yan et al. \(2016\).](#)

32

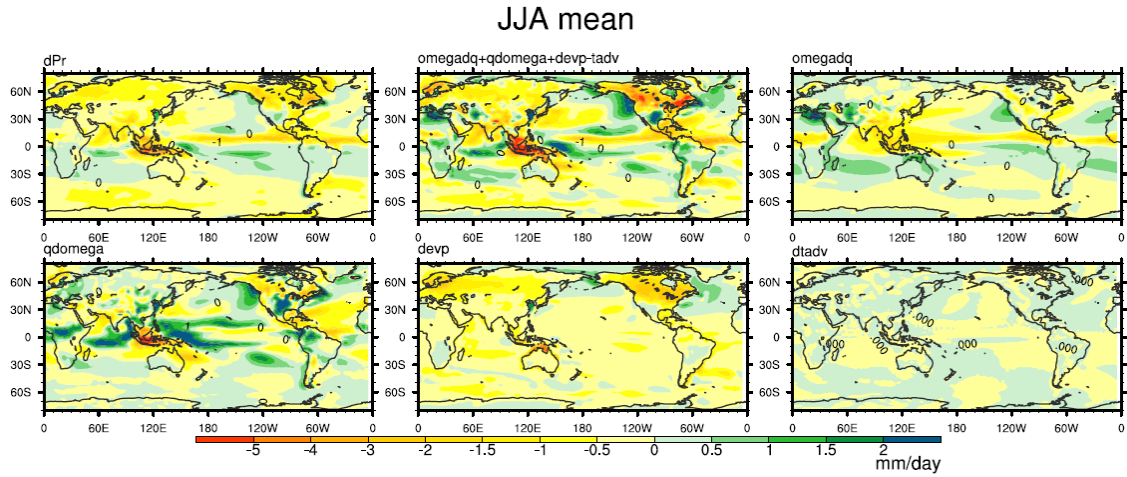
33



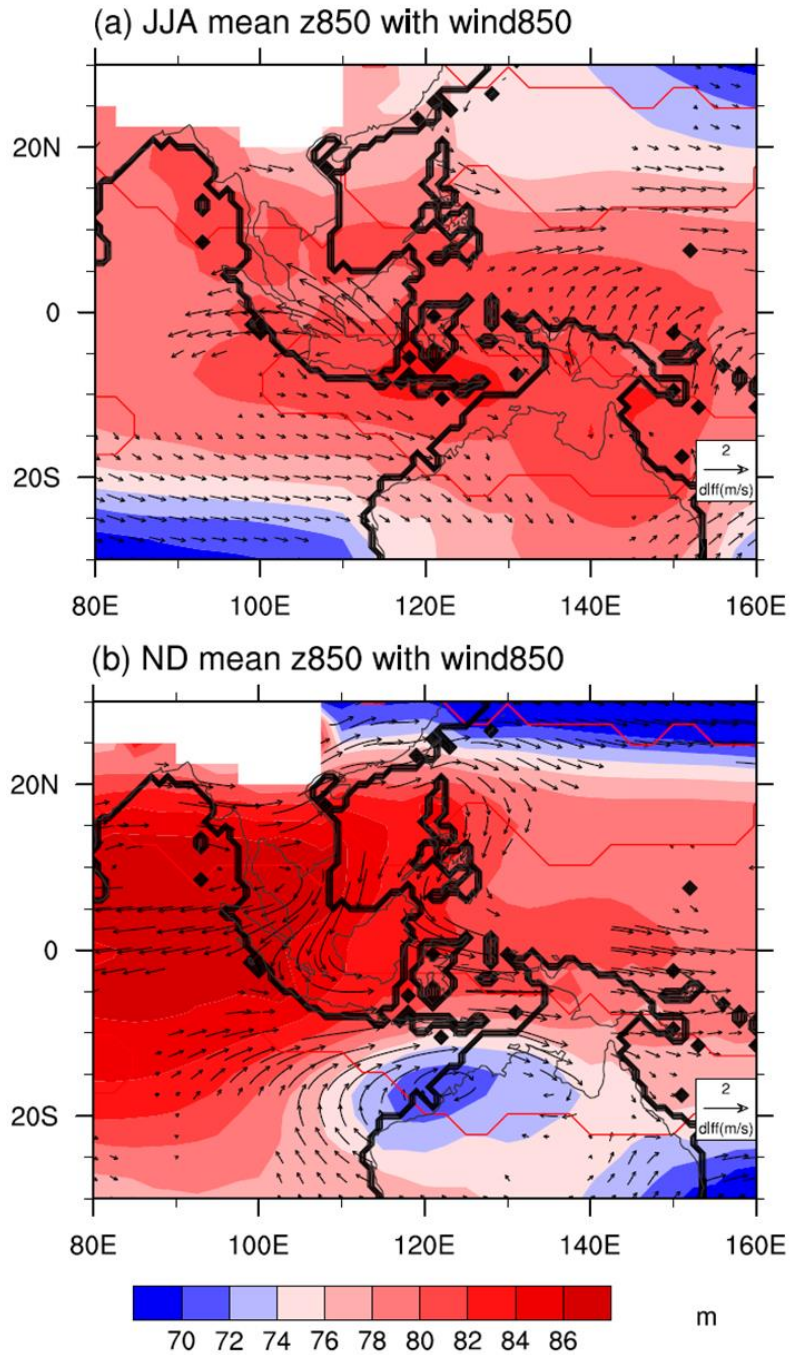
34

35 **Figure S2** Distributions of the land–sea mask and land-ice during the LGM. The land–sea mask
36 during the LGM is in red contour. The land-sea mask during the PI is in black contour. The land
37 ice-sheet is color-shaded. [Reprint of Fig. 1 in Yan et al. \(2016\).](#)

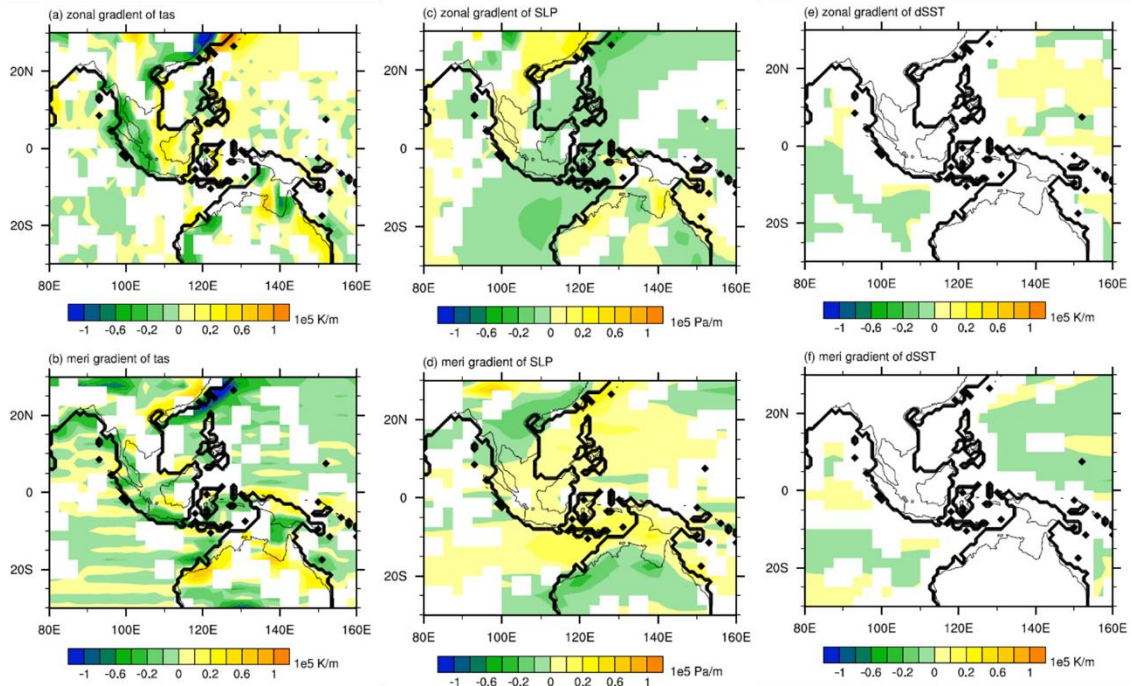
38



39
 40 **Figure S3** The JJA mean difference between LGME and piControl derived from 7MME. Shown
 41 are precipitation (top left), sum of each term (top center), thermodynamic term (top right),
 42 dynamic term (bottom left), surface evaporation (bottom center) and advection term (bottom
 43 right).
 44
 45



47
 48 **Figure S4** The (a) JJA mean, and (b) ND mean 850 hPa geopotential height (shading) with 850
 49 hPa wind (vector) difference between LGME and piControl. The red lines enclose the monsoon
 50 domains. The thick black lines denote the coastal lines in LGME [provided by CMIP5/PMIP3](#), and
 51 the thin black lines denote the coastal lines in piControl. Only those areas where signal-to-noise
 52 ratio exceeds one are plotted.
 53

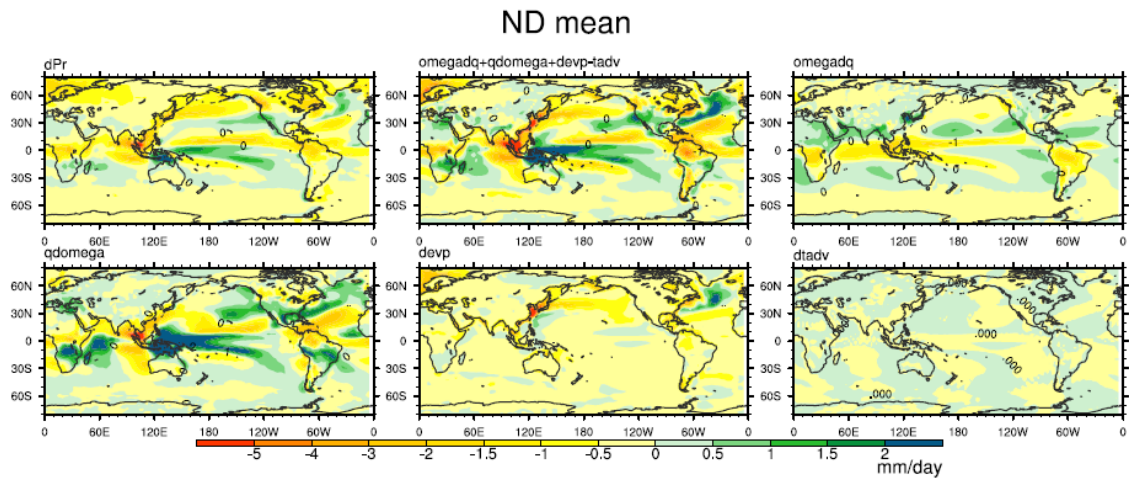


55

56 **Figure S5** The ND mean zonal (top panels) and meridional (bottom panels) gradient difference
 57 between LGME and piControl. (a)-(b) for surface air temperature anomaly, (c)-(d) for sea level
 58 pressure anomaly, and (e)-(f) for sea surface temperature anomaly. The thick black lines denote
 59 the coastal lines in LGME [provided by CMIP5/PMIP3](#), and the thin black lines denote the coastal
 60 lines in piControl. Only those areas where signal-to-noise ratio exceeds one are plotted.

61

62



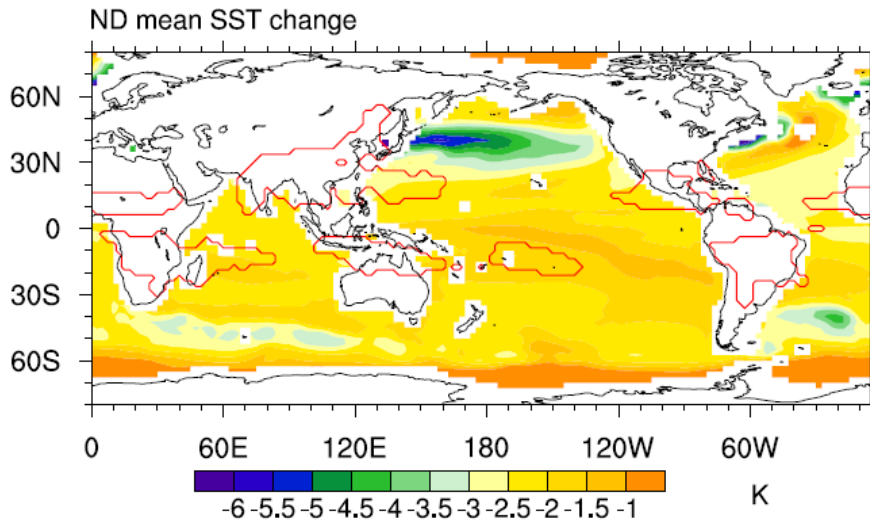
63

64

Figure S6 Same as Fig. S3, but for ND mean.

65

66

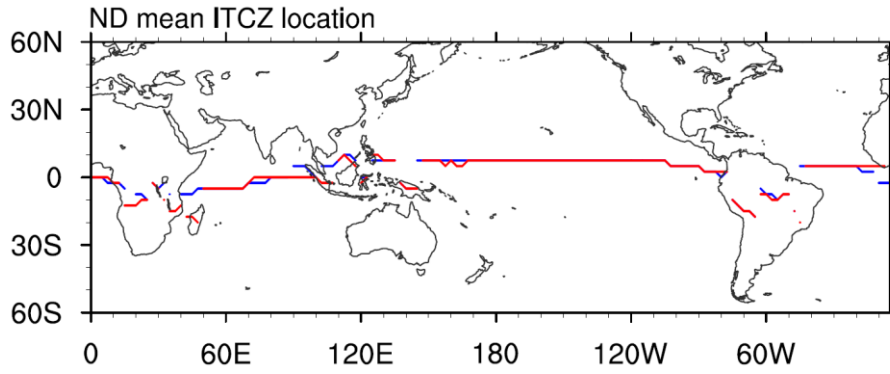


67

68 **Figure S7** The ND mean SST difference between the LGME and piControl. The orange lines
69 enclose the monsoon domains. Only those areas where signal-to-noise ratio exceeds one are
70 plotted.

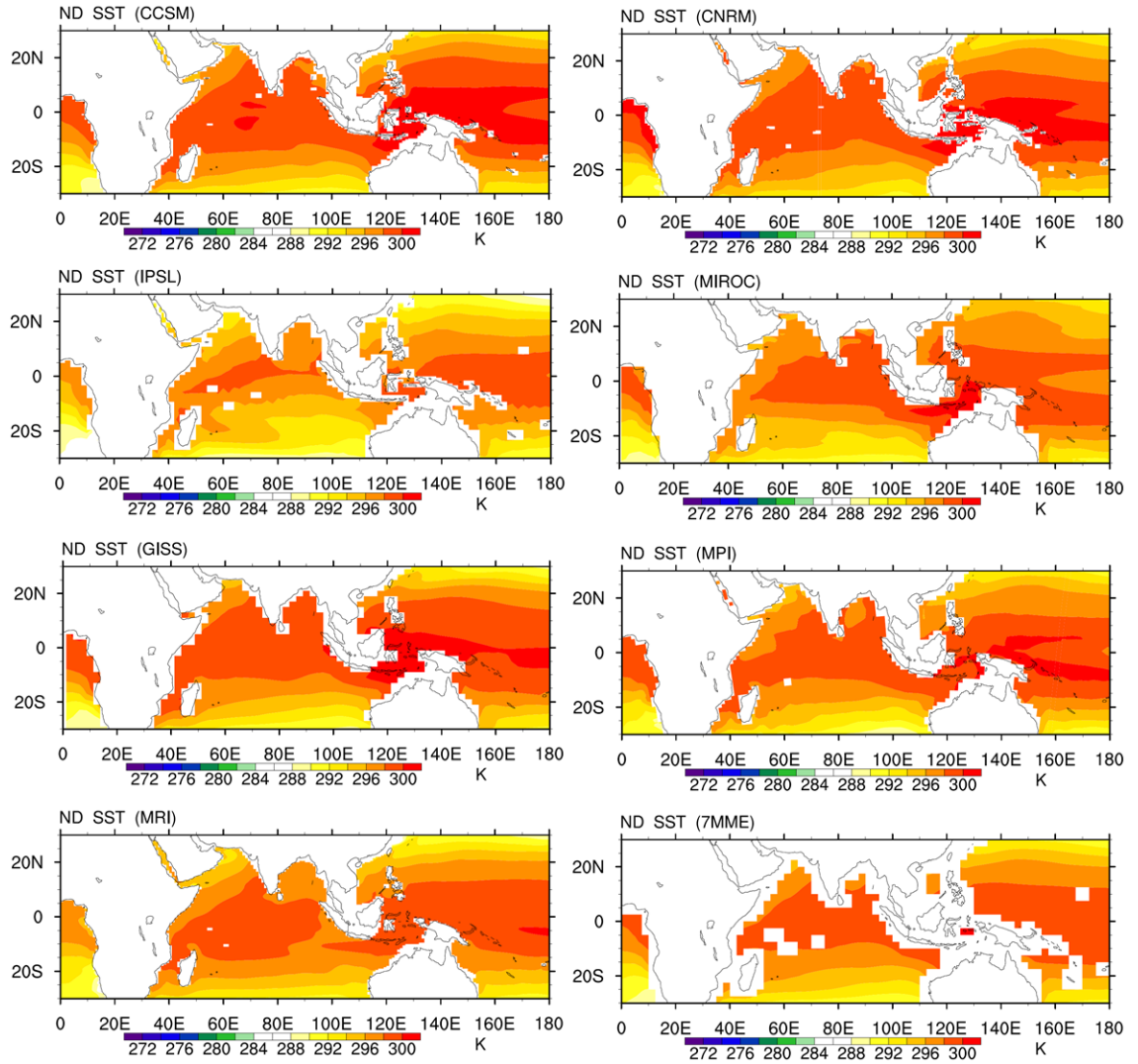
71

72
73
74
75
76



77
78
79
80
81

Figure S8 The 7MME ND mean ITCZ location defined by the meridional maximum precipitation between 20°S and 20°N. The red line indicates the position during the LGM and the blue line indicates the position during the PI.



82
83
84

Figure S9 ND mean SST in LGME derived from each model and 7MME.